THESIS

DESIGN, CONSTRUCTION AND COMMISSIONING OF AN ORGANIC RANKINE CYCLE WASTE HEAT RECOVERY SYSTEM WITH A TESLA-HYBRID TURBINE EXPANDER

Submitted by

Nicholas Cirincione

Department of Mechanical Engineering

In partial fulfillment of the requirements

For the Degree of Master of Science

Colorado State University

Fort Collins, Colorado

Fall 2011

Master's Committee:

Advisor: Daniel Olsen

Daniel Zimmerle
David Dandy

Copyright by Nicholas Ray Cirincione 2011

All Rights Reserved

ABSTRACT

DESIGN, CONSTRUCTION AND COMMISSIONING OF AN ORGANIC RANKINE CYCLE WASTE HEAT RECOVERY SYSTEM WITH A TESLA-HYBRID TURBINE EXPANDER

Issues surrounding energy are some of the most compelling subjects in the world today. With human's ever increasing need for energy, production must increase or consumption must be reduced to avoid an unsustainable long-term energy balance.

One part of the energy solution is low-temperature Organic Rankine Cycles (ORCs). ORCs can be utilized to produce power in mass quantity from a dedicated heat source such as a geothermal well. ORCs may also be utilized as a waste heat recovery system to generate power from a heat stream that is typically rejected to the environment. Low-temperature waste heat streams are ubiquitous as every internal combustion engine generates 55-75% of its total fuel energy as waste heat.

Efficiency of a waste heat recovery ORC system is strongly dependent on condensing temperature and expander efficiency. Condensing temperatures are typically kept low with an evaporative condensing unit. However, water consumption to increase energy production is becoming less tolerated.

To provide a means to conduct research around these issues, a waste heat recovery ORC test bed was designed and constructed. This thesis contains information

on construction and operation of the test bed with these features: R245fa working fluid, direct dry cooled condensing and a Tesla-hybrid turbine expander.

ACKNOWLEDGEMENTS

I would like to thank the entire staff of the EECL from the undergraduates to the director for their tireless enthusiasm to solve problems, answer questions and assist with construction of the system. Phillip Bacon and Kirk Evans have fundamental knowledge of the facility and the systems therein and were instrumental in getting the physical aspects of the system installed. Jason Golly and Adam Friss where always willing to lend a hand when more than 2 were needed. Jon Cosgrove worked endlessly to complete as much welding as possible before having to start an industry job. Thanks to Dean Gebhardt from Excel Energy for donating his time to finish what Jon couldn't get to.

Thanks to the 2009-2010 ORC senior design team, Owen Yamanaka, James Ignatius, Thomas Boileau and Vincent Vong for running full steam ahead on the project during their final semester. Always remember, "everything takes twice as long as you think it will".

Thanks to Mark Toukan of Toucan Design Inc. for letting us "borrow" his turbine for the better part of 2 years. I hope the discoveries made can aid you in furthering your technology and business.

Finally, I would like to thank Dan Zimmerle for his guidance which started before I even set foot in the EECL and continued throughout my entire time here. Dan never stops thinking and coming up with new ideas.

TABLE OF CONTENTS

ABSTRACT ii
ACKNOWLEDGEMENTS iv
LIST OF FIGURES viii
LIST OF TABLES x
LIST OF ABBREVIATIONS xi
1. Introduction 1
2. State of the Technology 4
2.2 The Rankine Cycle and Organic Rankine Cycle 4
2.3 Organic Working fluids 7
2.4 Expanders 9
2.5 Applications of ORCs 12
3. ORC Challenges 14
3.1 kW Scale Expanders and Associated Systems 14
3.2 Water Consumption 15
3.2.1 Dry Condensers and the Moving Condensation Point 15
3.3 High Level Design Decisions 19
4. Modeling 20
5. Experimental Equipment 23
5.1 Feed Pump 23
5.2 Vaporizer 24
5.2.1 Heat Source 27
5.2.1.1 Caterpillar G3516C 27
5.2.1.2 Waukesha VGF18GL 28
5.3 Expander 29
5.4 Condenser 30

5.5 Buffer Tank 31
5.6 Piping 32
5.6.1 Filter Dryer 33
5.7 Electrical Systems 33
5.7.1 National Instruments cRIO Data Acquisition (DAQ) and Control System 34
5.7.2 Pump Motor and Variable Frequency Drive (VFD) 35
5.7.3 Generator and Generator VFD 35
5.8 Sensors 36
5.8.1 Flow Meter 36
5.8.2 Temperature 37
5.8.3 Pressure Transducers 37
5.8.4 Speed Sensor 38
5.8.5 Water/glycol Flow Meter 39
5.9 Safety Systems 39
5.9.1 Safety Trip System 39
5.9.2 Refrigerant Leak Detection 41
5.10 Maintenance System 41
5.10.1 Carrier Vapormizer 2000 41
6. Experimental Procedures 42
6.11 Test Procedures 42
6.11.1 Preparations 42
6.11.2 Heat Source Engine Warm Up 43
6.11.3 WHR ORC System Operation 43
7. Results and Discussion 45
7.1 Commissioning: June 2011 45
7.1.1 Commissioning Results 45
7.2 Testing Day 1: July 21, 2011 46
7.2.1 Testing Day 1 Results 47
7.3 Testing Day 2: Oct 21, 2011 48
7.3.1 Testing Day 2 Results 49
8. Conclusions 53
8.1 Recommendations For Future Work 53

9. References 56
Appendix I - REFPROP Excel Model Spreadsheet 60
Appendix II - AspenTech Aspen Plus Annotated Flowsheet 61
Appendix III - Pro-E Model 62
Appendix IV - Vaporizer Specifications 64
Appendix V - Condenser Specifications 65
Appendix VI - Piping and Instrumentation Diagram 66
Appendix VII - Valve Configuration Table 67

LIST OF FIGURES

Figure 2-1: General schematic of Rankine cycle components and process flow. 4

Figure 2-2: P-h diagram of a typical conventional Rankine cycle with superheat. Arrows indicate direction of energy flow into or out of system. 5

Figure 2-3: P-h diagram of a typical organic Rankine cycle demonstrated with R245fa.... 6

Figure 2-4: Comparative P-h diagram of RC and ORC working at the same condensing temperature. Note increased vaporization temperature and pressure, overall energy flow and superheat required for the RC. 7

Figure 2-5: Vaporization pressure of various working fluids at 85 °C [22,23]. 9

Figure 3-1: General energy stream of large internal combustion engine. 14

Figure 3-2: Schematic of Rankine cycle using direct dry cooling. 16

Figure 3-3: Schematic of Rankine cycle using dry cooling and secondary cooling loop, commonly known as indirect dry cooling 17

Figure 3-4: High and low condensing temperature ORC with R245fa as the working fluid and heat input at 85 °C. 18

Figure 4-1: Cycle efficiency for R245fa versus condensate return temperature. 21

Figure 5-1: Vaporizer with spare individual plates not installed. 26

Figure 5-2: Vaporizer as installed with piping. 26

Figure 5-3: Caterpillar G3516C installed at the EECL. Photo courtesy of Colorado State University EECL. 28

Figure 5-4: Waukesha VGF18GL installed at the EECL. Photo courtesy of Colorado State University EECL. 28

Figure 5-5: Schematic of Tesla-type turbine. 29

Figure 5-6: Tesla-hybrid turbine as installed on WHR ORC test bed. 30

Figure 5-7: Condenser as installed on third floor roof at the EECL. 31

Figure 5-8: Two core Sporlan filter dryer. A four core version is used on the EECL ORC test bed. Photo courtesy of Parker Hannifin Corp, Sporlan Division..... 33

Figure 5-9: Main LabVIEW GUI on host computer..... 35

Figure 5-10: Micro Motion coriolis flow meter sensor (left) and transmitter (right)..... 37

Figure 5-11: Omega Engineering DRF-FR-24VDC frequency to voltage converter and Sensor Solutions Corp. gear tooth sensor. 39

Figure 5-12: Dedicated overspeed PLC, Koyo Click C0-02DD20D..... 40

Figure 7-1: Pump Speed, Flow Rate and Differential Pressure. Note differential pressure peaking at 0.5 MPa and flow rate dropping repeatedly while pump speed is constant. This indicates the pressure relief valve was opening repeatedly..... 48

Figure 7-2: System efficiency versus turbine RPM. Negative efficiency indicates the system was consuming more power than it was producing. The general shape of the efficiency curve is important indicating the turbine's highest efficiency is near 4000 RPM..... 52

LIST OF TABLES

Table 2-1: Non-exhaustive list of RC working fluids in industry and research 8

Table 2-2: Non-exhaustive list of ORC turboexpanders and positive-displacement expanders..... 10

Table 2-3: Example efficiencies of some PD machines..... 11

Table 4-1: Model constraints and assumptions..... 20

Table 5-1: Working fluid feed pump attributes. 24

Table 5-2: Electrical sources and sinks..... 34

Table 5-3: Control and data acquisition system components. 34

LIST OF ABBREVIATIONS

ACR	–	Air Conditioning and Refrigeration
DAQ	–	Data Acquisition
EECL	–	Engines and Energy Conversion Laboratory
EOS	–	Equation of State
GUI	–	Graphical User Interface
GWP	–	Global Warming Potential
ICE	–	Internal Combustion Engine
ODP	–	Ozone Depletion Potential
ORC	–	Organic Rankine Cycle
OTEC	–	Ocean Thermal Energy Conversion
P&ID	–	Piping and Instrumentation Diagram
PD	–	Positive Displacement
P-h	–	Pressure-enthalpy
RC	–	Rankine Cycle
VFD	–	Variable Frequency Drive
WHR	–	Waste Heat Recovery

1. Introduction

The 2010 World Energy Council survey indicates energy efficiency and renewable energies as two of the highest “need for action” issues on the world energy agenda [1]. The ever increasing thirst for energy for industrialized and developing countries alike is driving the need for action. With the increase in demand for energy comes increased greenhouse gas emissions and consumption of finite fuel sources. The world is heading towards a long term energy balance that cannot be sustained.

Waste heat recovery (WHR) systems can be part of the solution for increasing energy efficiency and generating renewable power. For example, the overall efficiency of an industrial process can be increased with a WHR system. WHR technologies can also be used to produce power from a dedicated heat source, and is considered a renewable energy that can be used to meet renewable portfolio standards in several states in the United States [2].

A key technology used to generate power from heat is the conventional steam Rankine cycle (RC) which is used where high temperature (>340 °C) heat is available [3]. Unfortunately, not all heat sources produce sufficiently high temperature heat required to drive a conventional steam Rankine cycle. Such temperatures are especially rare when considering waste heat. It is estimated 20-50% of industrial energy inputs are lost as waste heat and 60% of the losses are at low temperatures (<230 °C), which are not typically accessible to steam Rankine cycles [3]. Further, a large amount of low-grade

waste heat is produced from smaller sources, such as automobile engines, simply by the sheer number of sources.

The development of lower boiling point organic working fluids has provided an avenue for increased applications of RCs to low-temperature heat sources. Organic Rankine cycles (ORC), a Rankine cycle with an organic working fluid instead of water, allow utilization of heat for power generation from sources as low as 65 °C.

Sources of heat for ORCs may be either waste sources or dedicated sources. Examples of waste sources are industrial processes, biogas digesters configured as combined heat and power systems, internal combustion engines (ICE) exhaust and cooling systems and gas turbine exhaust. Example dedicated sources are ocean thermal energy conversion (OTEC), geothermal and solar collectors.

The technologies to build ORC systems were available as early as 1976. The economics of ORCs weren't favorable until the use of modified off the shelf refrigeration components lead to packaged systems [4]. It is estimated there were 30 commercial ORC plants built before 1984 with an output over 100 kW [5]. Large scale ORCs have been commercialized and deployed around the world in several of the aforementioned applications. However, there are still technological and economic challenges to wide acceptance of the technology to smaller applications in the less than 100 kW range. Smaller systems are important as there are many more sources of waste heat in this range of operation. To that end, the effort in this work was undertaken to create an environment to conduct research on sub-100 kW ORCs and collect preliminary results for one ORC configuration of working fluid and expander.

The research contained in this work focuses on two tasks:

1. Model, design and build a full-scale ORC test bed implementing a direct dry cooled condenser.
2. Commission a Tesla-hybrid turbine on the test bed with R245fa working fluid.

The test bed was constructed at Colorado State University's Engines and Energy Conversion Laboratory (EECL) in Fort Collins, Colorado, USA. The EECL has multiple heat streams at varying temperatures and capacities generated by the many onsite engines making for an ideal location for such a test bed.

2. State of the Technology

2.2 The Rankine Cycle and Organic Rankine Cycle

A basic RC consists of 4 processes as outlined below and shown in schematic form in Figure 2-1 and on a pressure-enthalpy (P-h) diagram in Figure 2-2.

1-2 Compression in a pump

2-3 Vaporization in a boiler

3-4 Expansion in an expander

4-1 Condensation in a condenser

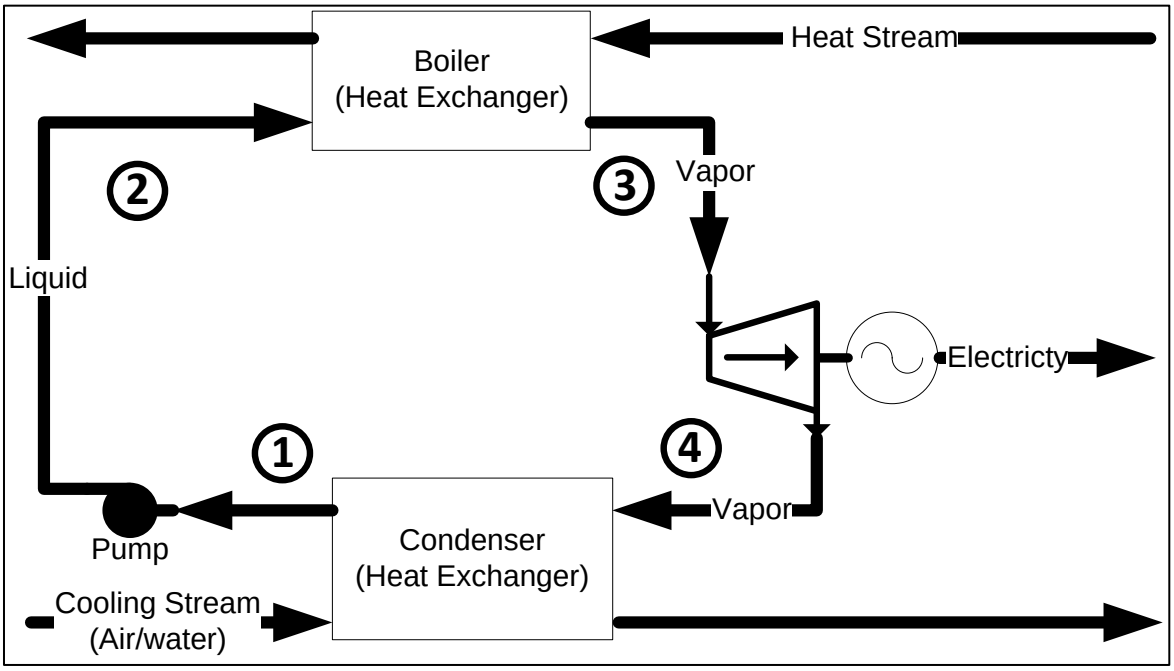

Figure 2-1: General schematic of Rankine cycle components and process flow.

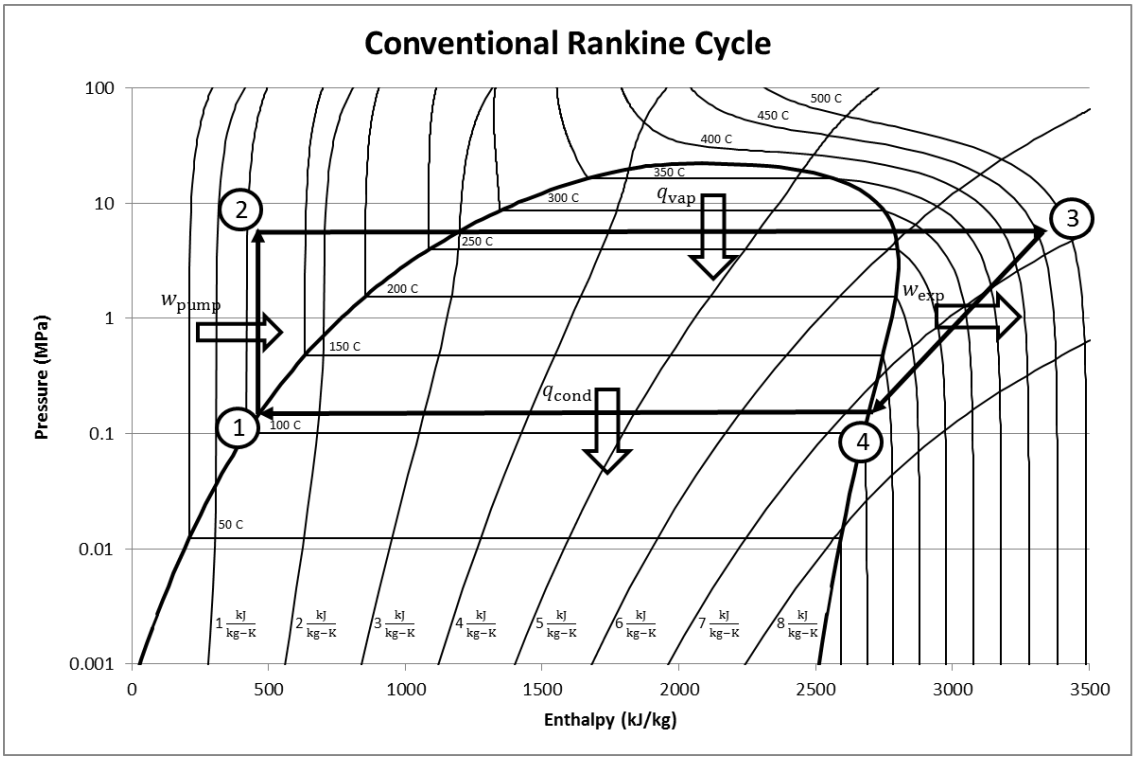

Figure 2-2: P-h diagram of a typical conventional Rankine cycle with superheat. Arrows indicate direction of energy flow into or out of system.

A steam power cycle is a specific Rankine cycle that uses water as the working fluid and produces electrical power as an output from the expander. For the purposes of this work, a conventional RC will be defined as using water (steam) as the working fluid while an ORC uses an organic (containing carbon) compound as the working fluid.

Organic working fluids commonly have lower vaporization temperatures than water and often exhibit a vapor saturation line with a less than or equal slope than the isentropic lines in the same vicinity when plotted on a P-h diagram as shown in Figure 2-3.

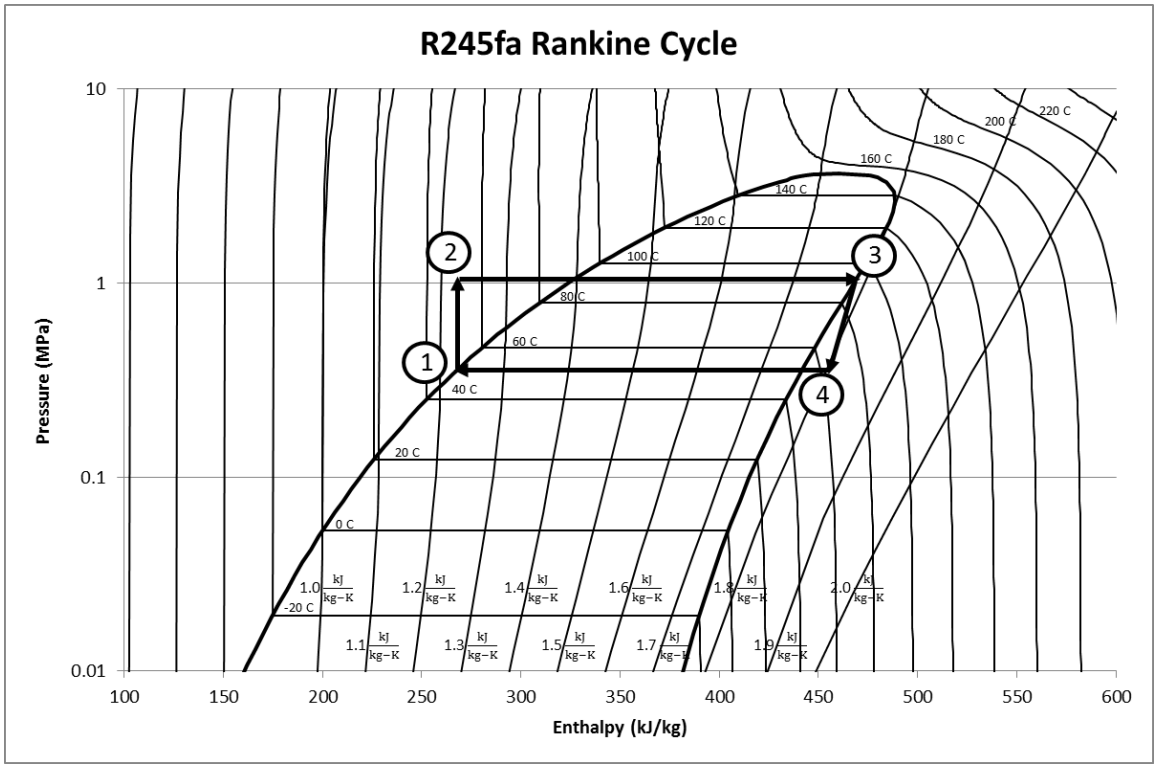

Figure 2-3: P-h diagram of a typical organic Rankine cycle demonstrated with R245fa.

The lower vaporization temperature of organic fluids allows the application of the RC to low-grade heat sources and the conventional RC becomes economically impractical at input temperatures below 370 °C [6]. The slope of the vapor saturation line in relation to the isentropes eliminates the need for a high level of superheat. Working fluids with a vapor saturation line with a smaller slope than the isentropes in the area are considered “dry” because at the end of expansion, state 4, the working fluid is a superheated vapor. In a properly designed RC, vapor exits the expander at 100% quality, that is, state 4 is outside the vapor dome. If the working fluid crosses into the vapor dome during expansion, blade erosion and considerable stress can occur on the expander. Figure 2-3 shows no superheat is required to operate the ORC with a dry working fluid, whereas Figure 2-2 shows a significant amount of superheat is required to

eliminate condensate before the expander exhaust in a conventional RC. A comparative P-h diagram of a conventional RC and an ORC is shown in Figure 2-4. The main advantage of the ORC is it allows the use of ubiquitous lower temperature heat sources to drive the power cycle.

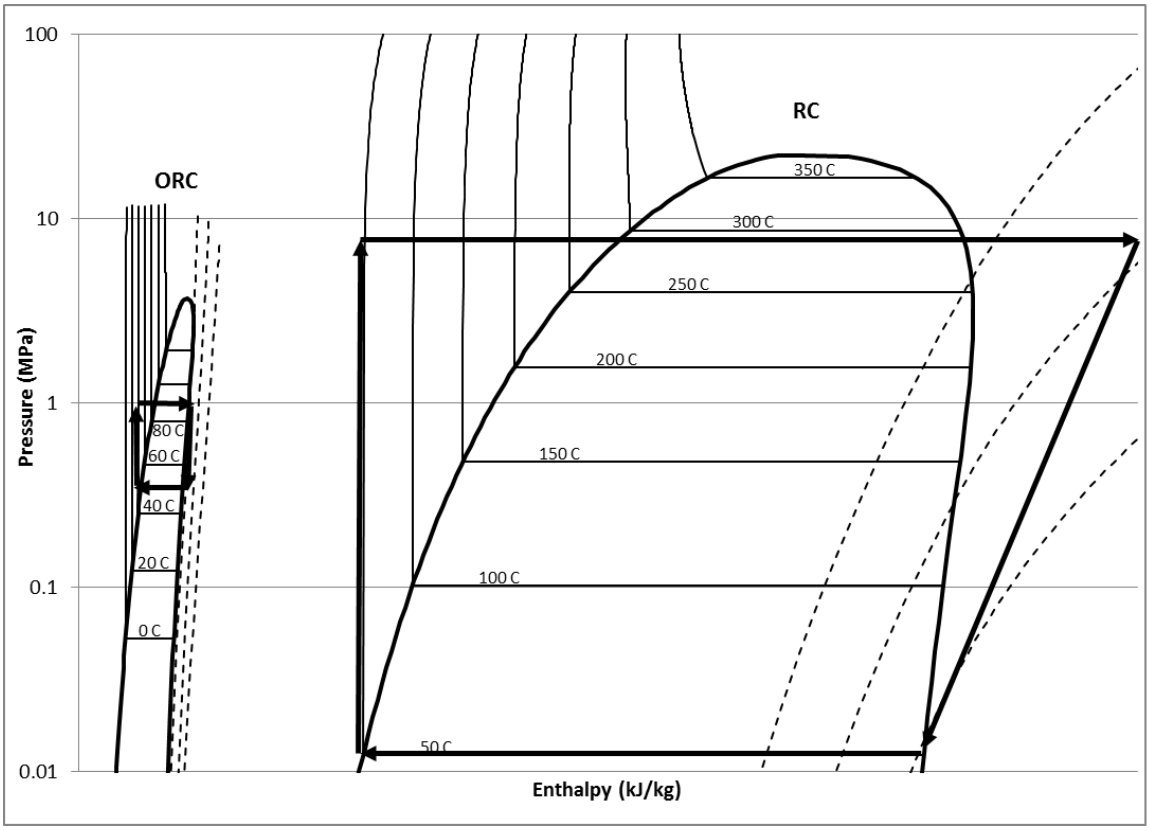

Figure 2-4: Comparative P-h diagram of RC and ORC working at the same condensing temperature. Note increased vaporization temperature and pressure, overall energy flow and superheat required for the RC.

2.3 Organic Working fluids

Organic working fluids have been developed that have high molecular weight and specific heat, low or zero ozone depletion potential (ODP), low global warming potential (GWP) and low flammability.

Much research has been conducted on the effect of working fluid selection as it applies to Rankine cycles [7–14]. Working fluids studied include water, ammonia, chlorofluorocarbons, hydrofluorocarbons , hydrochlorofluorocarbons, carbon dioxide and many other materials. Many fluids have attractive thermophysical properties, but are quickly ruled as unfavorable for anything other than research due to flammability, toxicity, lack of availability, cost, required working pressures or are subject to phase-out due to environmental considerations. Table 2-1 gives examples of working fluids currently being used in industry and for research.

Table 2-1: Non-exhaustive list of RC working fluids in industry and research
Sources: Company websites and noted citations.

Study/Company	Working Fluid	Power Output
Ormat [15]	Isobutane	11.3 MW
Turboden	Solkatherm	1-7 MW
Cryostar [16]	R245fa, R134a	500 kW – 12 MW
Pratt and Whitney	R245fa	280 kW
General Electric	R245fa	125 kW
Freepower, UK	n-Hexane	6*, 60*,85*,120 kW
Tri-O-Gen	Toluene	60 – 165 kW
Nelson, Cummins [17]	R245fa	60 kW
Teng, AVL [18]	Ethanol	11.6 kW*
Electratherm	R245fa	65 kW
Ener-g-rotors	Proprietary	40-60 kW
Infinity Turbine	Varies	10-30 kW
Freymann et al.,BMW [19]	Water	10 kW*
Endo et al., Honda [20]	Water	2.5kW*
Oomori and Ogino, Toyota [21]	R123	400 W*

*Prototypes only or not commercially available as of May 2011.

Figure 2-5 shows vapor pressure for working fluids in Table 2-1 plus three other common ORC fluids at 85 °C, the temperature available for this work. All fluids except R245fa and Solkatherm were eliminated from consideration due to aforementioned reasons. Vaporization pressures above 1.03 MPa requires higher-pressure ratings for

equipment which increase costs significantly. Pressures below atmospheric, required to vaporize water and Toluene at 85 °C, are more costly due to additional equipment required to eliminate air from the closed system. Solkatherm was unknown to the researcher during the fluid selection phase therefore was not considered. The efficiency of R245fa is studied in Section 4. A lower ODP and GWP organic fluid with higher cycle efficiency is being developed to replace R245fa and is discussed in Section 8.1.

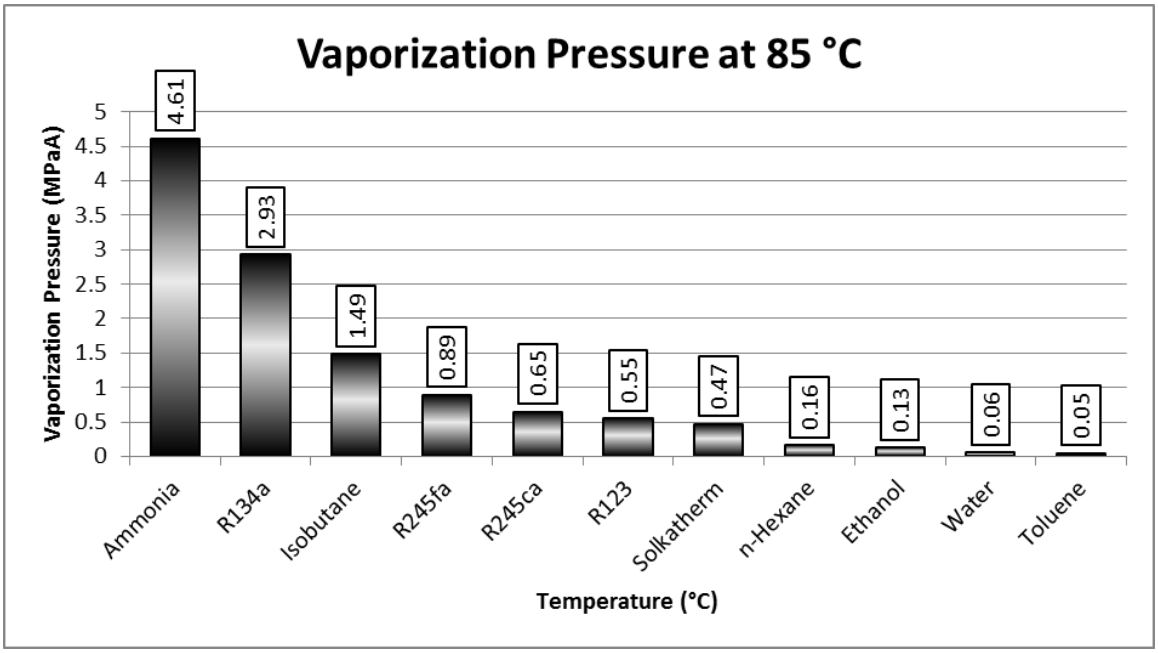

Figure 2-5: Vaporization pressure of various working fluids at 85 °C [22,23].

2.4 Expanders

The efficiency of an ORC system is strongly dependent on the efficiency of the expander [24,25]. Expander selection for specific operating temperatures, working fluid, and expansion ratio is important. Generally, expanders can be categorized into two primary clusters: turboexpanders and positive displacement (PD) machines.

Turboexpanders are most often used in large scale plants while PD machines are used in smaller plants as shown in Table 2-2. Turboexpanders work at rotational speeds as high as 50,000 RPM and typically exhibit peak efficiencies in the 60-90% range. The high speed of turboexpanders requires a sophisticated design and manufacturing effort and increased component cost. Special bearings, seals and lubrication systems are often required. Turboexpanders do not work well at off-design conditions and are damaged by working fluid condensing before the exhaust.

Table 2-2: Non-exhaustive list of ORC turboexpanders and positive-displacement expanders. Sources: Company websites and noted citations.

Study/Company	Expander Type	Power Output
Turboexpanders		
Ormat [15]	Axial, multi-stage	11.3 MW
Turboden	Axial	1-7 MW
Cryostar	Radial Inflow	500 kW – 12 MW
Pratt and Whitney	Radial Inflow	280 kW
General Electric	Radial Inflow	125 kW
Freepower, UK [27]	Radial Inflow 2 or 3 stage	6*, 60*,85*,120 kW
Tri-O-Gen	Radial Inflow	60 – 165 kW
Nelson, Cummins [17]	Radial Inflow	60 kW*
Teng, AVL [18]	Centrifugal	11.6 kW*
Positive Displacement Expanders		
Electratherm	Twin-Screw	65 kW
Ener-g-rotors	Gerotor	40-60 kW
Infinity Turbine	Screw	10-30 kW
Eneftech	Scroll	10-30 kW
Freymann et al.,BMW [19]	Axial Piston	10 kW*
Endo et al., Honda [20]	Swash plate axial piston	2.5kW*
Oomori and Ogino, Toyota [21]	Scroll	400 W*

*Prototypes only or not commercially available as of May 2011.

PD machines operate at slower speeds and exhibit higher expansion ratios than similarly sized turboexpanders. The slower speed reduces the need for higher cost rotating components and reduces manufacturing costs in areas such as balancing. These factors contribute to lower expander cost for PD machines versus turboexpanders. PD

expanders show lower peak efficiencies than turboexpanders, but work well through a range of operating conditions. As concluded by Badr et el. [26], PD expanders are best suited for small waste heat systems.

Isentropic efficiencies are not available for all expanders mentioned in Table 2-2 as many are proprietary designs. However, Table 2-3 gives some experimental efficiencies of PD machines from previous studies.

Table 2-3: Example efficiencies of some PD machines.

Study	Expander Type	Isentropic Efficiency (%)
Tahir et el. [28]	Rotary Multi-Vane	43.1-48
Badr et el. [29]	Rotary Multi-Vane	73
Ng et el. [30]	Screw	73-85
Badr et el. [29]	Screw	70
Mathias/Johnston et el. [24,31]	Gerotor	45-85
Mathias/Johnston et el. [24,31]	Scroll	50-83
Lemort et el. [32]	Scroll	68

Early ORC systems utilized modified large scale refrigeration compressors running in reverse flow to function as an expander. For example, Pratt and Whitney's PureCycle® is based off the Carrier Corp 19XR centrifugal chiller compressor working in reverse [33]. The compressors, benefitting from decades of research by the refrigeration industry, were technologically advanced and exhibited high efficiencies. Along with the benefits of advanced technology, Pratt and Whitney could rely on Carrier's existing supply chain. The leap from a chiller system to an ORC for power generation required little technical and business development. For these reasons, large scale modified refrigeration compressor based systems were first to market. Now that large scale ORC

systems have made significant inroads to acceptance, the focus is turning towards smaller systems for widespread dissemination.

2.5 Applications of ORCs

The term “waste heat recovery” can be used to describe utilization of any heat typically rejected to the environment. Viable sources are numerous in breadth and number of installations. Examples include industrial processes, incinerators, gas turbines, internal combustion engines, steam boiler return flows and furnace exhaust [34]. A thorough review of applications of industrial waste heat recovery is given by Johnson and Choate in [3]. Heat can be exchanged directly to process fluids, structures or water supplies. The waste heat can also be converted to electricity using a thermodynamic cycle. ORCs are used to convert low-grade heat into electricity when there is no direct use of heat on site. The power can be used to offset electricity consumption on site or, if power in excess of site loads is generated, exported to the local utility. WHR cycles emit no incremental emissions, other than those incurred in manufacturing of capital equipment, and require no additional fuel for power generation.

ORCs are also used to generate power from dedicated low temperature heat sources such as geothermal, OTEC, biomass and low-temperature solar concentrators [35–38]. ORC technology has been commercialized by companies such as General Electric, Ormat, Turboden, Pratt and Whitney, Electratherm, Infinity Turbine, GMK, Adoratec, Koehler-Ziegler, Cryostar, Freepower and Tri-o-gen [16,39]. System sizes for

WHR and dedicated applications range from under 1 kW on automotive ICEs [21], to multi-unit systems generating several megawatts [33].

3. ORC Challenges

3.1 kW Scale Expanders and Associated Systems

Small scale ORCs for power generation from low grade heat can be applied to a multitude of waste heat streams. Although per unit output is minimal, small waste heat streams are ubiquitous. Large ICEs are a source of multiple waste heat streams as shown in Figure 3-1.

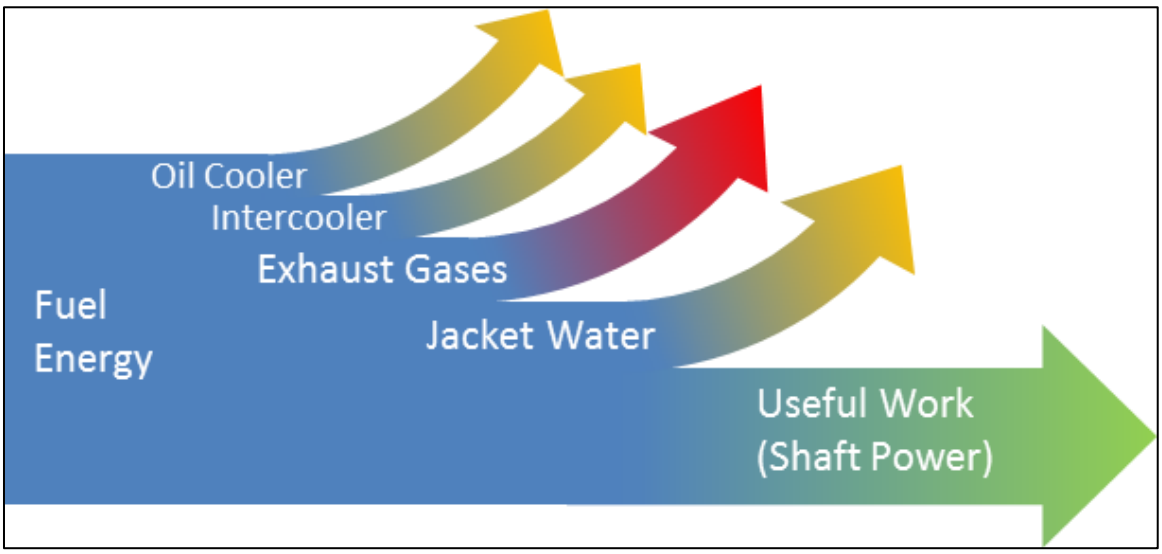

Figure 3-1: General energy stream of large internal combustion engine.

Roughly 55-75% of all fuel energy input to an ICE is rejected as waste heat. Generally, smaller ICEs, typical of automotive or small generation applications, are less efficient than larger ICEs designed for distributed power applications. Applications of ORCs applied to larger ICEs do exist, typically in the form of a bottoming cycle utilizing

exhaust heat. However, widespread integration as part of every ICE, whether stationary or mobile, would be ideal, and ideally such deployments would economically utilize both high temperature exhaust and low temperature water/glycol streams.

Studies have applied ORCs theoretically and physically to several small waste heat streams and proven their effectiveness [17,18,20,21,40–44]. It is also noted that few of the expanders and even fewer complete systems from those studies are available commercially as shown in Table 2-2. The dissemination of small scale ORCs is small and needs significant marketing, economic and technical development.

3.2 Water Consumption

Every Rankine cycle operates between two temperatures. One temperature is the heat source where heat is absorbed and the other is a lower temperature where heat is rejected. If the lower temperature decreases, and the system is designed for it, the cycle will operate more efficiently. Evaporative cooling is used in many cases to decrease and maintain the heat sink temperature in low humidity, high ambient temperature locations such as the United States desert southwest. There is increasing concern over the consumption of water for evaporative cooling which puts energy production in direct competition with water for agricultural and human consumption needs [45].

3.2.1 Dry Condensers and the Moving Condensation Point

In solving the ecological and political water problem, another challenge is created. With some tradeoffs, using a heavily finned dry cooler can be utilized as the low

temperature condensing side of an ORC as one solution to eliminate water consumption. Dry coolers cannot control the condensing temperature they impart on an ORC as well as an evaporative condenser when ambient air temperature increases. Extra fans can be activated to minimize thermodynamic efficiency losses, but total system efficiency may be decreased due to the fan load on the electrical system.

Direct and indirect condensing methods must also be considered. The direct method condenses the working fluid directly in the condenser. The indirect method uses a secondary cooling loop to remove heat from the working fluid in the condenser. Direct and indirect systems are shown schematically in Figure 3-2 and Figure 3-3.

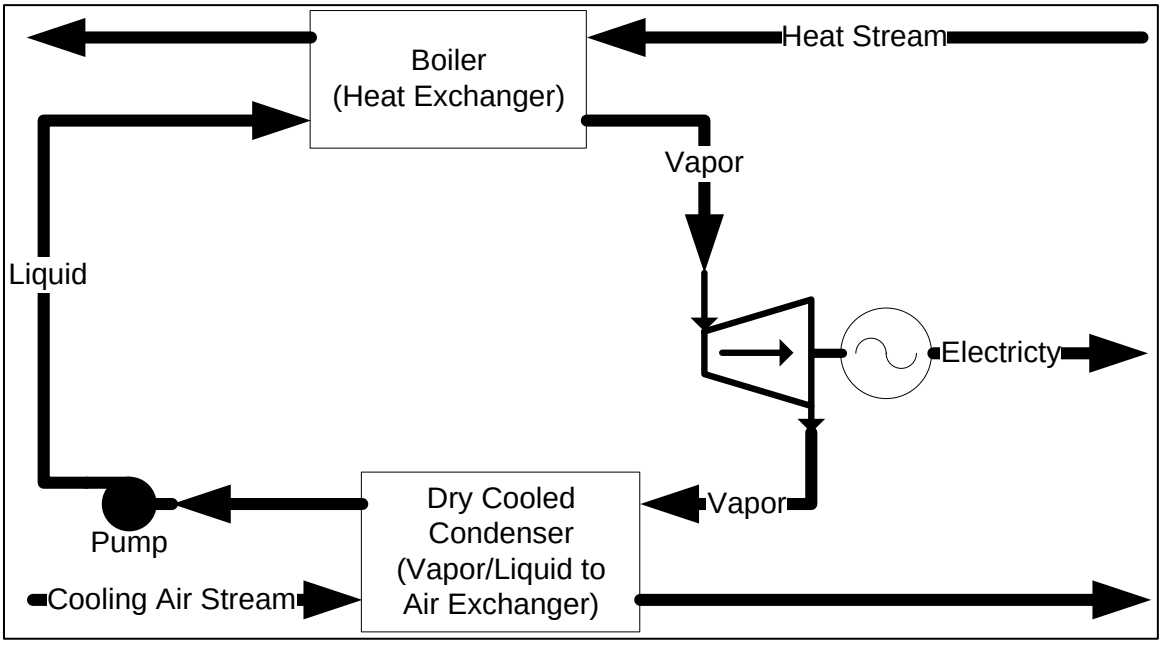

Figure 3-2: Schematic of Rankine cycle using direct dry cooling.

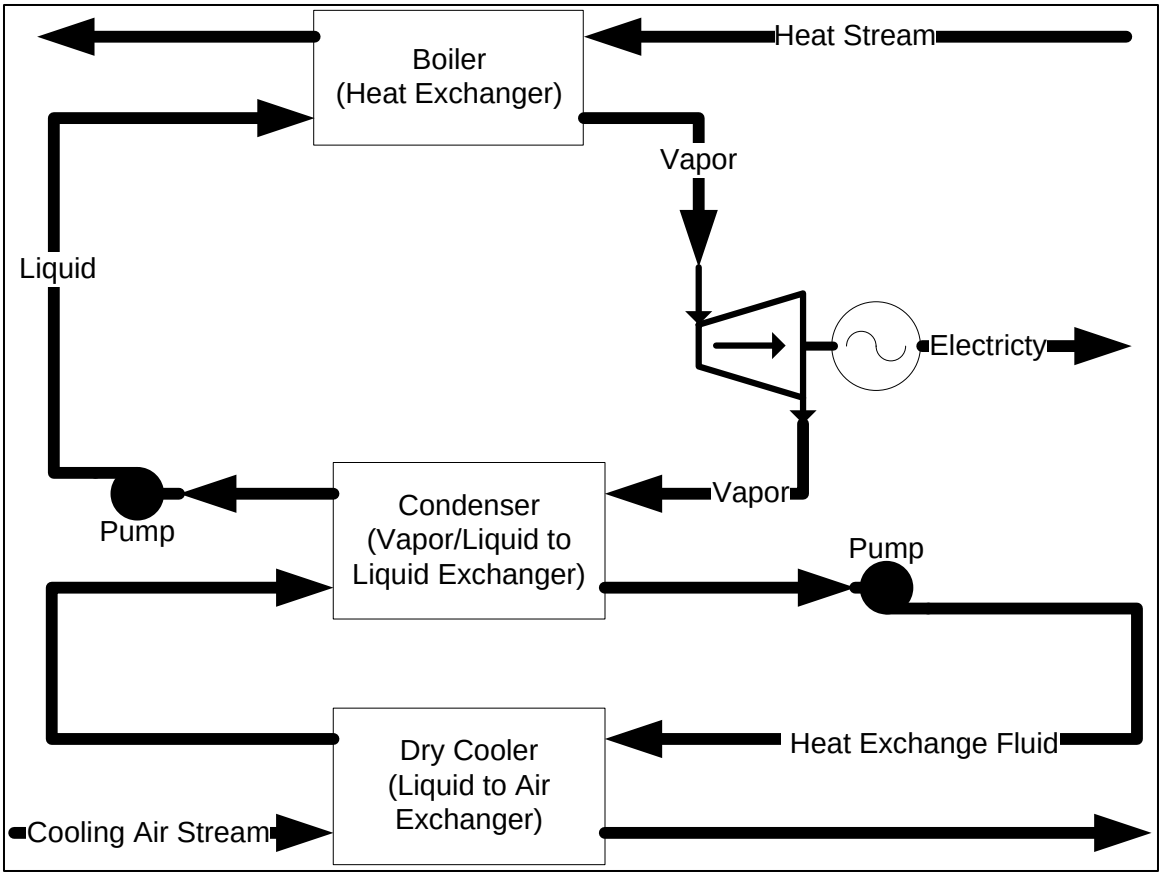

Figure 3-3: Schematic of Rankine cycle using dry cooling and secondary cooling loop, commonly known as indirect dry cooling

A finned dry condenser has to be larger than its equivalent duty evaporative cooled condenser. If a direct condensing method is used, an increase in system volume is realized which increases the required working fluid charge. With expensive organic working fluids, the increased cost can be significant. A trade off can be made to use a secondary cooling loop with a liquid to liquid heat exchanger at the monetary cost of the extra pump, heat exchanger and the efficiency lost using the pump and having two heat exchanger pinch points.

If a direct dry cooler is used as the cold side of a RC, the condensing temperature will fluctuate with ambient air temperature and air mass moved by the fans. Most

expanders designed into RCs have fixed expansion ratios optimized to work between a specified pressure differential. The inlet pressure and backpressure at the expander is directly related to the heat input and rejection temperatures. If a system is designed to work well at the upper operating pressure of the dry condenser, it is difficult for the expansion device to take advantage of the lower pressure at its exhaust when lower ambient temperatures are observed. Figure 3-4 shows a P-h diagram of an ORC with R245fa as the working fluid operating between two different condensing temperatures.

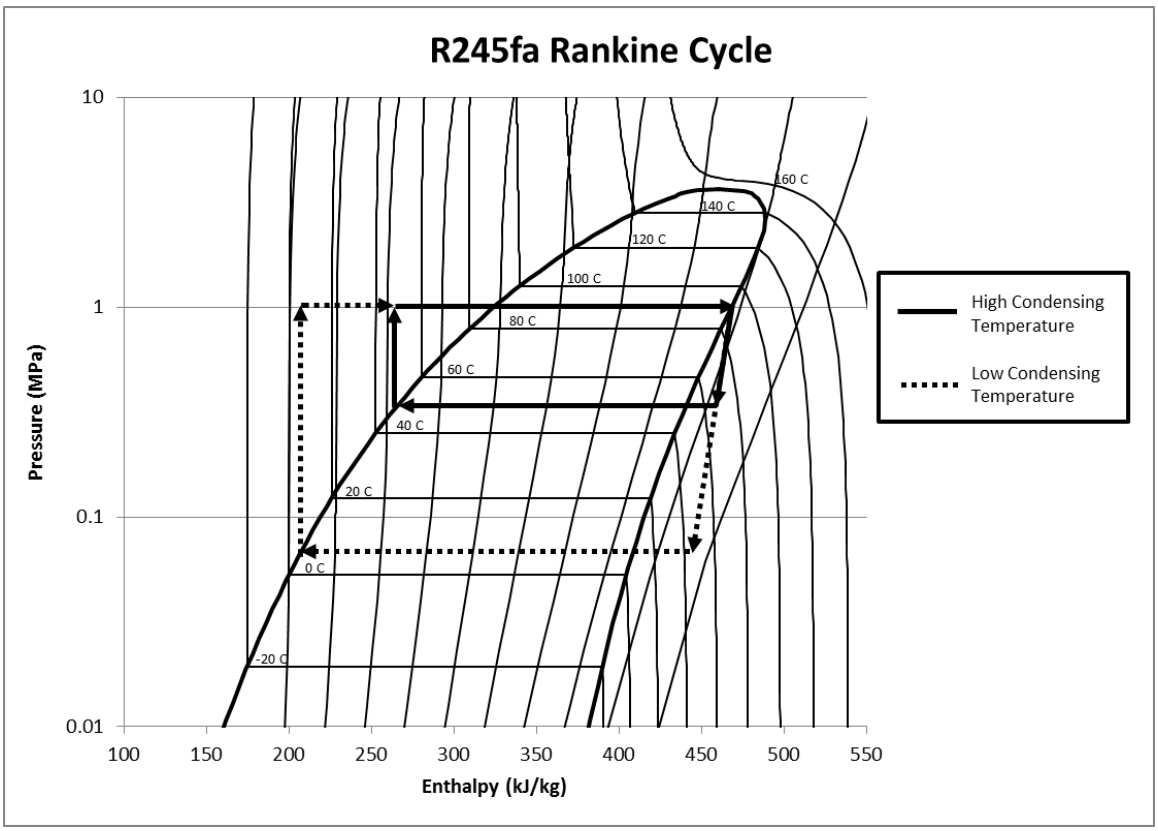

Figure 3-4: High and low condensing temperature ORC with R245fa as the working fluid and heat input at 85 °C.

In Figure 3-4 note the increase in expansion and associated enthalpy at the lower condensing temperature. One way to take advantage of the lower condensing

temperatures is with a variable geometry expansion device. If an expander could take advantage of the increased expansion that occurs at lower condensing temperatures and associated pressures, the efficiency of an ORC system could be increased by as much as 19.5% over an annual cycle as concluded by Zimmerle and Cirincione [46].

3.3 High Level Design Decisions

The goal for the system described here was to create an environment to address the challenges outlined above. To accomplish that, a direct dry cooled ORC with an output limit of 30 kW was designed. The direct cooling of the working fluid in the condenser keeps costs low as a secondary cooling loop is not needed. The dry cooling method allows the condensing temperature and pressure to fluctuate with ambient temperature. A variable expansion device is yet to be identified for experiments on the test bed. However, one future goal is to confirm the performance modeling of fixed and variable expansion devices presented by Zimmerle and Cirincione in [46] and generate a compelling argument for the development of smaller variable expansion ratio devices.

4. Modeling

As mentioned in the introduction, one of the primary tasks for this work was to commission and characterize an experimental Tesla-hybrid turbine running as the expander of an ORC. The turbine was provided by Toucan Design Inc. of Boulder, CO, USA and was the starting point of the thermodynamic and physical system models. Other constraints were dictated by the operating environment at the EECL. Constraints and assumptions shown in Table 4-1 were placed on the thermodynamic model.

Table 4-1: Model constraints and assumptions.

Constraint	Affects	Values
Direct Dry Cooling	Condensing Temperature	55 to 15 °C
Direct Dry Cooling	Condensing Pressure	Varies with working fluid
Available Glycol Temperature	Vaporizing Temperature	85 °C
Turbine Isentropic Efficiency	Power Generation	75%
Turbine Expansion Ratio	Cycle Efficiency	Infinitely Variable
Pump Isentropic Efficiency	Power Consumption	75%

Thermodynamic modeling of the ORC to determine performance of working fluid was completed in Microsoft Excel using REFPROP [22] to calculate thermodynamic properties. A standard 75% isentropic efficiency was placed on the pump and turbine. As mentioned in section 2.3, there are many working fluids to be considered and several could produce better system efficiency numbers than R245fa, but are not safe for the environment or the operating facility. A plot of system efficiency versus condensate return temperature for R245fa is shown in Figure 4-1.

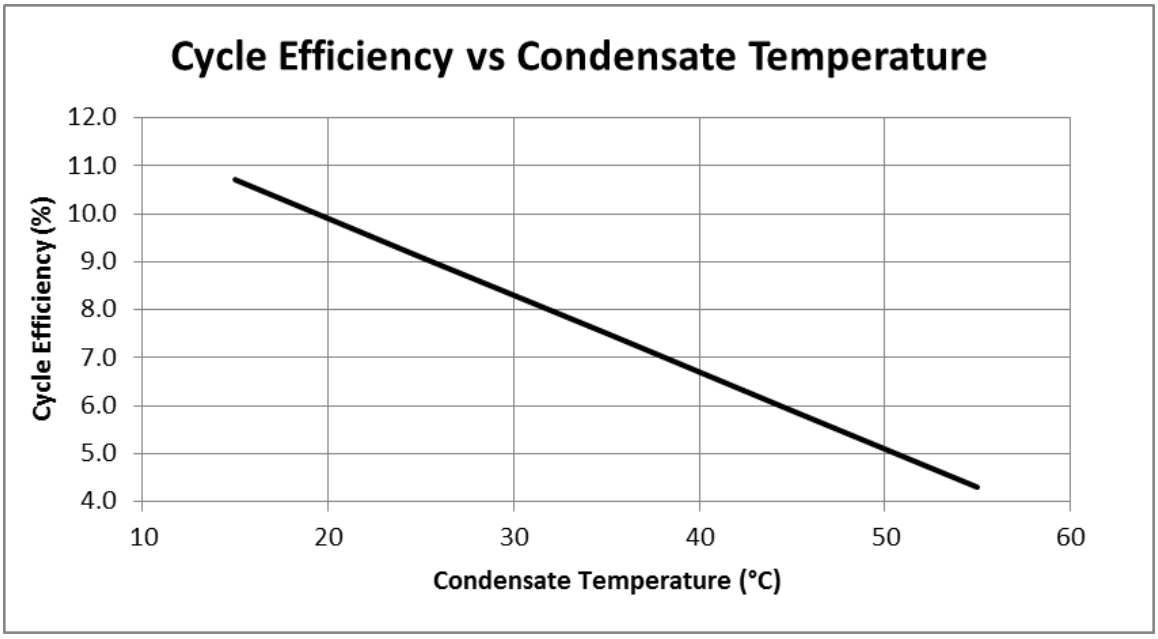

Figure 4-1: Cycle efficiency for R245fa versus condensate return temperature.

A system flow rate was not initially known as this is a function of how the working fluid interacts with the turbine. After R245fa was selected as the working fluid, studies were run by Toucan Design Inc. to determine the maximum flow rate the turbine could theoretically handle. Flow rate was then applied to the model so overall heat transfer rates could be established and system sizing completed. The final excel spreadsheet is shown in Appendix I with the condenser temperature set at 50 °C, the maximum design condition.

Aspen Plus by AspenTech was used to confirm the Excel model and add more detail by considering piping loses caused by elevation changes and pipe friction. Aspentech can also implement numerous equations of state (EOS) onto the model. A Peng-Robinson EOS was used to verify the REFPROP Excel model. An annotated flowsheet from the Aspentech simulation is shown in Appendix II.

Once flow rates and heat duties were confirmed, bids were requested for the vaporizer and condenser. As bids came in from various suppliers, the heat exchangers were modeled in AspenTech Exchanger Design and Rating to confirm the quoted heat duties and other performance characteristics.

In parallel with the thermodynamic model, a physical model was developed in Pro-E to determine where each piece would spatially fit into the EECL. The model is shown in Appendix III.

A detailed electrical schematic was also created in Microsoft Visio before system wiring began.

5. Experimental Equipment

All equipment is installed at the EECL. The main skid is located on the ground floor while the condenser is located on the third floor roof. The piping to transport the water/glycol from the heat source engines to the main skid is located along the basement ceiling of the EECL.

5.1 Feed Pump

A positive displacement pump was desired for increasing working fluid pressure and generating the working fluid flow rate. Positive displacement pumps are characterized by the ability to create high pressure over a wide range of operating points. In a dynamic research environment, this flexibility is desirable.

A Blackmer SGL 1.5 sliding vane pump with PTFE encapsulated Viton seals and a built in pressure relief valve was procured. The non-standard PTFE seals were required for material compatibility with R245fa refrigerant. The pump is directly coupled to a 2 horsepower motor with a Lovejoy L90 coupling. Table 5-1 below shows the relevant attributes of the pump.

Table 5-1: Working fluid feed pump attributes.

Attribute	Value
Manufacturer	Blackmer
Model	SGL 1.5
Maximum Outlet Pressure	3.62 MPa
Maximum differential pressure	1.03 MPa
Seals	PTFE Encapsulate Silicon/HNBR
Minimum Temperature	-34 °C
Rated Speed	1750 RPM
Rate Capacity at Speed	121 L/min

Early testing showed the PTFE O-Rings did not seal correctly from the factory and leaked working fluid to the atmosphere. Neoprene seals deemed safe when used with the working fluid at temperatures near the condensate return of the system were installed and the leak corrected. It is also noted the vane pump made a very audible clicking sound when running at slow speeds. The noise is believed to be caused by “vane chatter” as explained by Badr et el. [47].

5.2 Vaporizer

The thermal constraints of the vaporizer could be met by a number of different heat exchanger styles. Shell-and-tube heat exchangers to meet a 250 kW duty were cost prohibitive to the project and the size of an adequately sized shell-and-tube heat exchanger was quite large which would require a substantial increase in refrigerant charge. However, shell and tube heat exchangers impart a relatively small pressure drop on the working fluid. They primarily rely on surface area to transfer heat between the hot and cold fluids.

Plate heat exchangers meet the cost constraint and are compact in size with minimal internal volume/duty ratios. The downside is they create relatively large pressure drops as the fluids flow through narrow corrugated passages to increase turbulence, and in turn, the heat transfer coefficient. Fully-brazed plate heat exchangers are the lowest cost of the plate family, but are inflexible if increased duty is required for a future project.

An ITT Standard WP26 semi-brazed plate and frame heat exchanger was acquired for the application. PTFE rings seals are required for material compatibility with R245fa. A semi-brazed plate and frame heat exchanger is compact and expandable by adding more plates if a higher duty is required in the future. R245fa flows in the brazed cavities being in contact with a minimal amount of gasket surface reducing the chance of leaking expensive working fluid to the atmosphere. Appendix IV contains the detailed specifications for the purchased vaporizer.

Figure 5-1 and Figure 5-2 show the vaporizer with the spare individual corrugated plates and the vaporizer as installed with all piping connected.

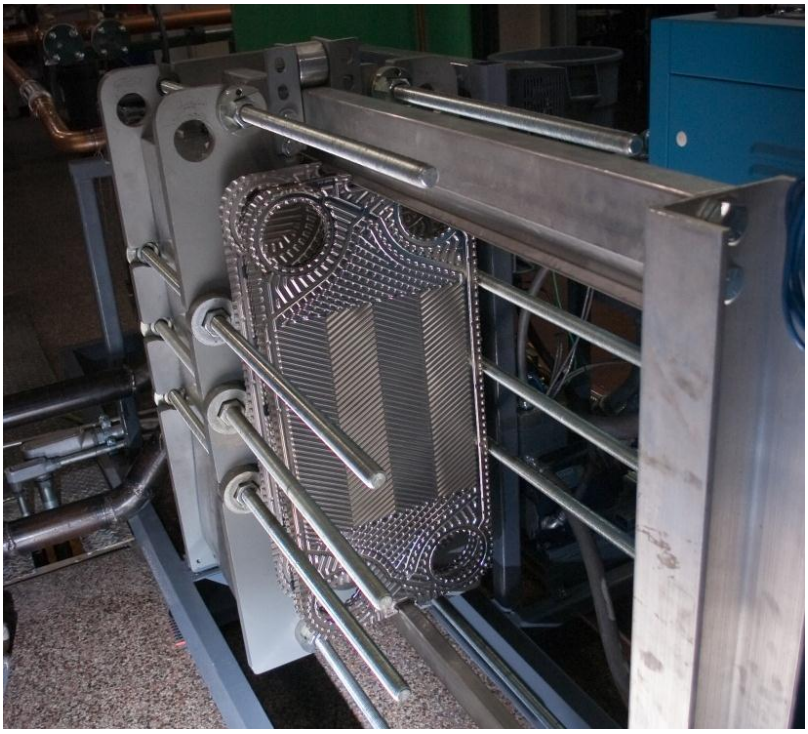

Figure 5-1: Vaporizer with spare individual plates not installed.

Figure 5-2: Vaporizer as installed with piping.

5.2.1 Heat Source

The EECL has two research engines that generate a high enough temperature water/glycol stream to vaporize R245fa in flow rates significant to drive the ORC. Both engines are connected to the same cooling system making it easy to capture heat from either with one set of piping. The utilization of exhaust gases as a waste heat stream was not part of the current project, but could be the subject of future work.

5.2.1.1 Caterpillar G3516C

The Caterpillar G3516C is a 16 cylinder, 4 stroke, 69 liter, lean burn natural gas engine. The G3516C rejects a total of 826 kW at approximately 92 °C to the water/glycol cooling loop at full load. An additional 989 kW is rejected via exhaust gases at 474 °C. The installed engine at the EECL can be seen in Figure 5-3.

Figure 5-3: Caterpillar G3516C installed at the EECL. Photo courtesy of Colorado State University EECL.

5.2.1.2 Waukesha VGF18GL

The Waukesha VGF18GL is a 6 cylinder, 4 stroke, 18 liter, lean burn natural gas engine. The VGF18GL is specified to reject a total of 230 kW at approximately 85 °C to the cooling loop. In the EECL installation, the jacket water temperature can be controlled up to 90 °C. Previous tests on the VGF18GL at the EECL revealed 194 kW of energy being rejected to the water/glycol loop. This is not enough energy to run the designed ORC at full capacity, however, data collected at these conditions are still valuable. The installed engine at the EECL can be seen in Figure 5-4.

Figure 5-4: Waukesha VGF18GL installed at the EECL. Photo courtesy of Colorado State University EECL.

5.3 Expander

An experimental Tesla-hybrid turbine was installed as the expander. Tesla turbines, known as friction, multiple-disk, shear force, or boundary-layer turbines, work off viscous effects of a fluid passing between closely spaced surfaces of the rotor pack. A Tesla turbine schematic is shown in Figure 5-5.

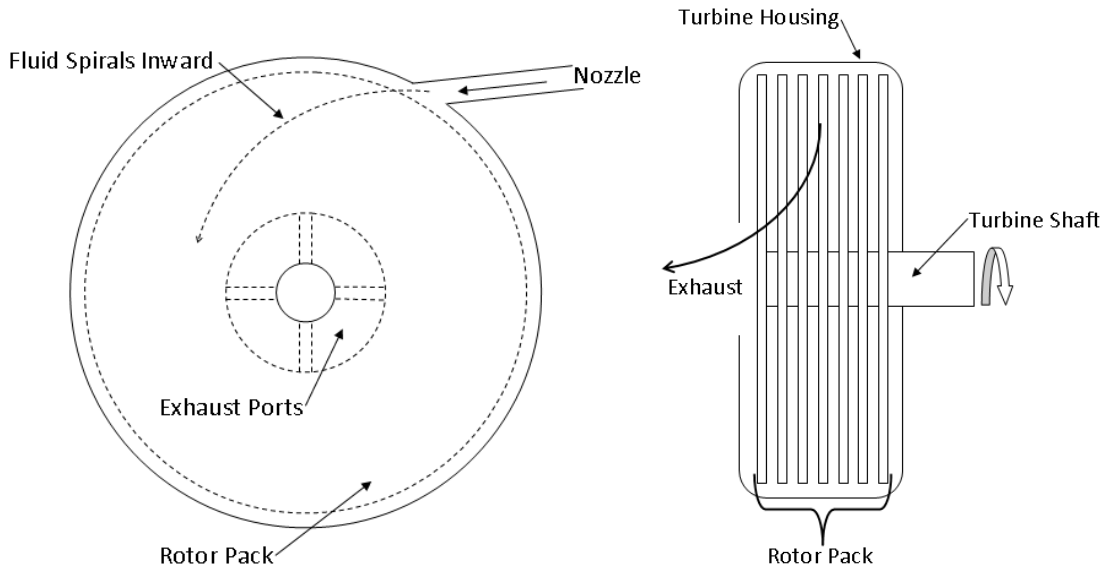

Figure 5-5: Schematic of Tesla-type turbine.

Nikola Tesla (1856-1943) patented his namesake turbine in 1913 [48]. The technology never caught on and, within a few years, interest dropped. In the late 1940's a renewed interest produced many theoretical and empirical studies right up until present [49–51]. Rice's theoretical studies point to a maximum isentropic efficiency of 65% [52], however, empirical studies have seen a range of 14-49% [53].

The turbine for the current work is the result of development undertaken by Toucan Design Inc. of Boulder, Colorado (Figure 5-6) on a hybrid, or modified Tesla

design. Recent improvements to the hybrid turbine have seen isentropic turbine efficiencies above 70% when run as a steam expander exhausting to atmospheric conditions. The 70% takes into account parasitic losses in power transmission from the turbine to the generator and power electronic losses. This work represents the first known experimental work using a Tesla turbine expanding organic working fluids for a RC application. Turbine design continues under the direction of Mark Toukan, president and director of the engineering efforts at Toucan Design Inc.

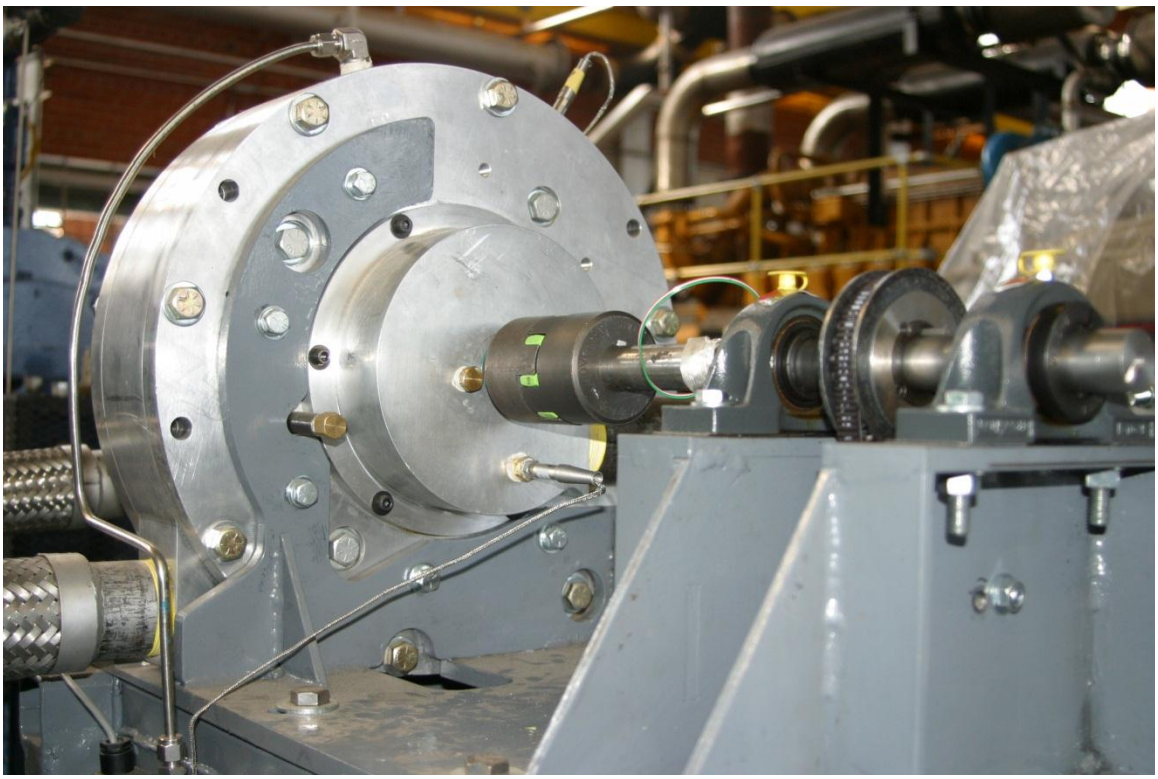

Figure 5-6: Tesla-hybrid turbine as installed on WHR ORC test bed.

5.4 Condenser

As stated in the introduction for this work, a direct, dry condensation method was employed to create a system that consumed no water. The condenser acquired is a 4 fan induced draft unit from Dry Coolers Inc. The dimensions and specifications are

shown in Appendix V. The unit was supplied to the EECL from Dry Coolers Inc. and the manufacturer was Guntner U.S. LLC. A Tempco TEC-9300 control unit came installed on the unit to cycle the fans on and off as a function of the outlet temperature of the condensate. The condenser as installed on the third floor roof of the EECL is shown in Figure 5-7.

Figure 5-7: Condenser as installed on third floor roof at the EECL.

5.5 Buffer Tank

The buffer tank serves to dampen fluctuations in the ratio of vapor to liquid working fluid due to ambient temperature changes and transient operating conditions. Without the buffer tank volume, an increase in the working fluid flow rate could cause the pump to run dry before the system can reach steady-state equilibrium. The buffer

tank chosen is a 302.8 liter, ASME certified steel tank rated to a working pressure of 1.38 MPa.

5.6 Piping

The constraints for piping consisted of handling 1.38 MPa at 100°C. Refrigeration systems are typically built from air conditioning and refrigeration (ACR) copper tubing. ACR tubing has low impurities in the base material and is sealed at the factory to eliminate contamination and corrosion during transportation and storage. ACR tubing was deemed excessively expensive and unnecessary for the current work. Carbon steel piping was sufficient in schedule 40 weight as was copper type M tube. An economic comparison was conducted including the cost for outsourced labor as a certified welder was not available for steel piping. Copper tubing could be soldered together by staff on hand, offsetting the increased material cost.

Type L copper tubing was sourced and Harris Products Group Stay-Brite (ASTM B32 Sn96) and Bridgit (ASTM B32 HB) solder were used for all permanent (non-threaded) connections. The increased cost from Type M to Type L tubing was acceptable for the increased safety factor and to allow the piping system to be used at higher pressures if required in the future. Typical refrigeration systems are brazed together for strength of the joints. The current system does not display the high pressures seen by a refrigeration system and the weakest soldered joints are rated to 1.9 MPa at 121 °C, sufficient for this project.

5.6.1 Filter Dryer

A filter dryer is required to remove impurities, particles and moisture from the working fluid to limit corrosion of the system from the inside out. A four core Sporlan C-19213-G shell with RCW-48 cores and a FS19200 secondary filter was installed at the inlet of the pump. A two core version is shown in Figure 5-8.

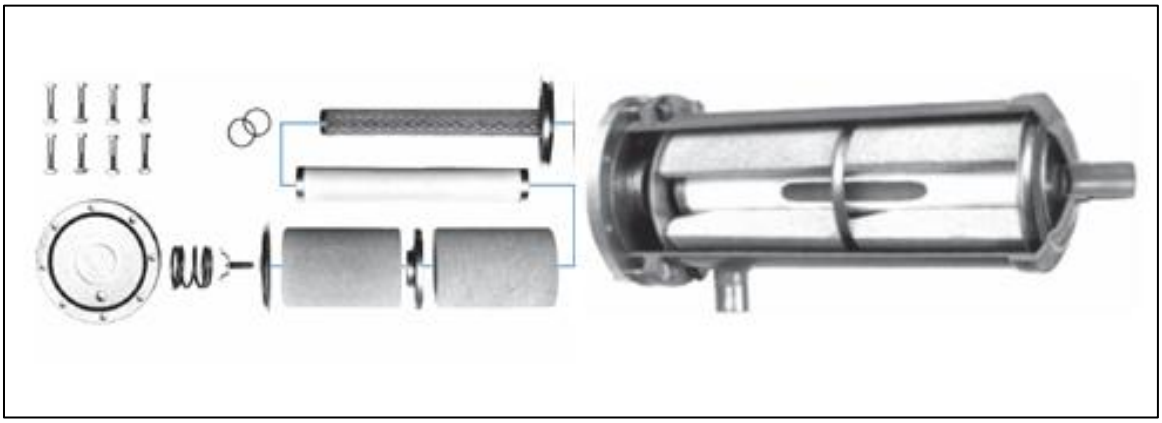

Figure 5-8: Two core Sporlan filter dryer. A four core version is used on the EECL ORC test bed. Photo courtesy of Parker Hannifin Corp, Sporlan Division.

5.7 Electrical Systems

Several electrical buses are required to operate the ORC as shown in Table 5-2 below.

Table 5-2: Electrical sources and sinks.

Item	Power Source/Sink
Pump	480V 3ϕ
Condenser Fans	480V 3ϕ
Generator	480V 3ϕ
Leak Detection System	120V 1ϕ
Network Router	120V 1ϕ
Digital I/O System	24 VDC
480V Breaker Shunt Trips	24 VDC
Turbine Bypass Valve Actuator	24 VDC
cRIO Control System	24 VDC
Programmable Logic Controller	24 VDC
Speed Sensor	24 VDC
Pressure Transducers	24 VDC
Flow Meter	24 VDC

5.7.1 National Instruments cRIO Data Acquisition (DAQ) and Control System

Monitoring, control and data logging are accomplished with the National Instruments cRIO platform. Table 5-3 shows the modules of the system.

Table 5-3: Control and data acquisition system components.

Component	QTY	Function/Specifications
NI cRIO-9074	1	Integrated Chassis and Controller
NI 9211	2	4-Channel 14 S/s, 24-bit, ±80mV Thermocouple Module
NI 9207	1	16-Channel (8 ±21.5mA) (8 ±10V) Analog Input Module
NI 9263	1	4-Channel 100 kS/s, 16-bit, ±10V, Analog Output Module
NI 9421	1	8-Channel 24V Logic, 100 µs, Sinking Digital Input Module
NI 9472	1	8-Channel 24V Logic, 100 µs, Sourcing Digital Output Module

The cRIO controller is programmed with LabVIEW and interfaces with a host graphical user interface (GUI) running on a network connected computer. The GUI is shown in Figure 5-9.

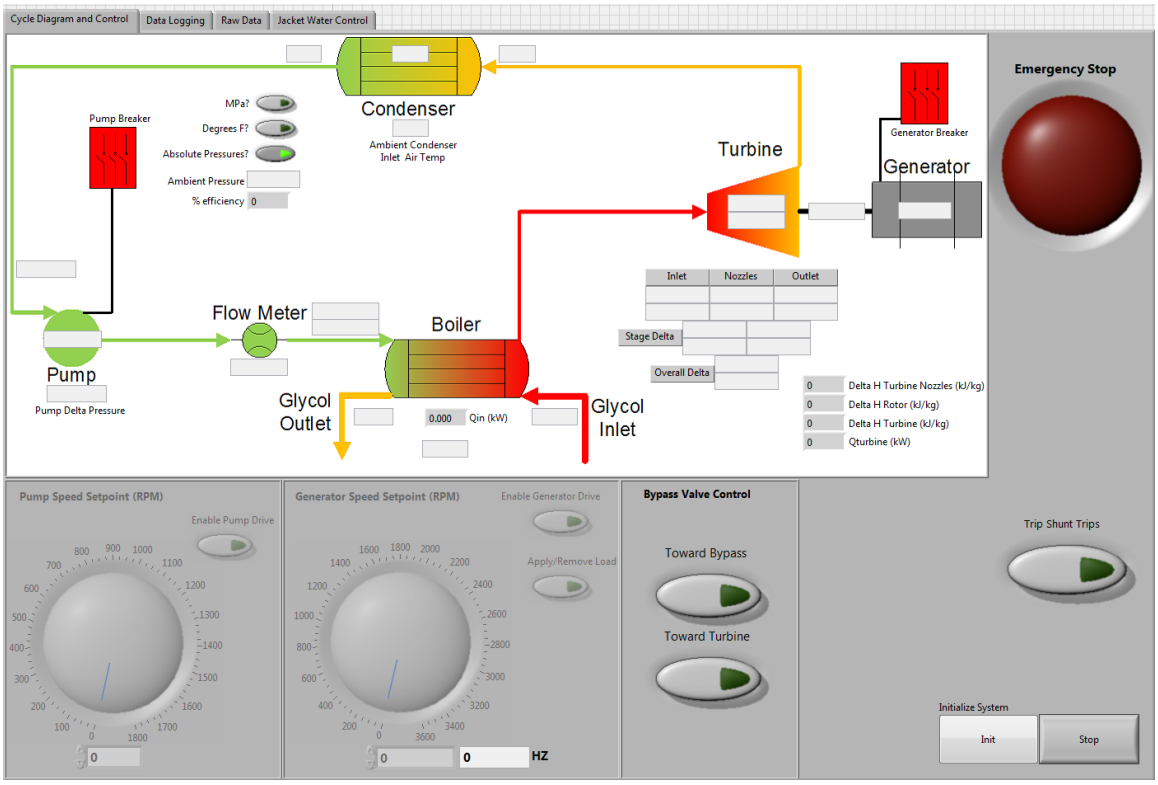

Figure 5-9: Main LabVIEW GUI on host computer.

5.7.2 Pump Motor and Variable Frequency Drive (VFD)

A Siemens Sinamics G120 2.2 kW VFD was used to drive the 1.5 kW,1725 RPM, Leeson (model C6T17DB40D) pump motor. The VFD consists of a PM240 (model 6SL3224-0BE22-2UAO) power module and a CU240E control unit (model 6SL3244-0BA10-0BA0). The VFD speed setpoint is set via a 0-10 VDC analog signal and the unit returns an instantaneous power consumption value to the DAQ system through a 0-10 VDC signal.

5.7.3 Generator and Generator VFD

Turbine load is achieved through coupling of the turbine via a Gates Corporation Poly Chain GT Carbon belt and pulleys to an asynchronous motor used as a generator.

The motor is connected to the building 480 V, 3 phase system through a regenerative VFD. Typically, extensive power electronics are needed to phase synchronize a generator to a grid connected load system. The Siemens PM250 power module has an option for regenerative capabilities with no additional external hardware. The motor load can be infinitely varied up to the full capacity of the VFD and the power generated flows to the facility power system. The need for costly additional hardware and a load bank is avoided.

The VFD selected for this duty is a Siemens Sinamics G120, 30 kW, PM250 power module (model 6SL3225-0BE33-0AA0) and a CU240E control unit (model 6SL3244-0BA10-0BA0). The VFD is coupled to a General Electric 22 kW,3560 RPM, asynchronous motor (model 5K284AD115). The VFD speed setpoint is set via a 0-10 VDC analog signal and the unit returns an instantaneous power consumption value to the DAQ system through a 0-10 VDC signal. This value is scaled in the DAQ system to indicate when power is being consumed or produced with a positive or negative number respectively.

5.8 Sensors

Signals for monitoring, control and logging for further analysis are obtained through several sensors and sent to the DAQ system.

5.8.1 Flow Meter

A Micro Motion coriolis flow meter, sensor model F050S322CQBAEZZZZ and transmitter model 2700R12BBAEZZZ, measures the working fluid mass flow rate at the

outlet of the pump. This flow rate value is transmitted as a scaled 4-20 mA signal to the DAQ system. Figure 5-10 shows the two flow meter components.

Figure 5-10: Micro Motion coriolis flow meter sensor (left) and transmitter (right).

5.8.2 Temperature

Thermal signals are obtained through two means. Eight T-type thermocouples are used in locations shown in the Piping and Instrumentation Diagram (P&ID) in Appendix VI. The Micro Motion flow meter provides an additional temperature point at its location at the outlet of the pump and is sent as a scaled 4-20 mA signal to the DAQ system.

5.8.3 Pressure Transducers

Five Futek PMP300, 0-1.38 MPa gauge, 4-20 mA output, pressure transducers monitor the working fluid pressure at locations shown in the P&ID in Appendix VI. Each transducer is mounted with a thermocouple to determine the state of the working fluid.

Absolute pressure is determined by offsetting gauge pressure with an ambient pressure measurement from a Rosemount 1151 pressure transducer which is part of the plant control system at the EECL. The data from the ambient pressure transducer is transmitted as a shared variable over Ethernet and is read by the main LabVIEW host program.

5.8.4 Speed Sensor

Turbine rotational speed is directly measured with a gear tooth sensor from the 30 tooth pulley coupled to the output shaft of the turbine. The sensor is a Sensor Solutions Corp. model M12-18ADSA-OCT21 single channel and receives power from and sends signals to an Omega Engineering DRF-FR-24VDC frequency to voltage converter. Both are shown in Figure 5-11. The sensor generates a 0-15 VDC square-wave pulse train which is converted to a 0-5 VDC signal by the DRF-FR module. The 0-5 VDC signal is sent to the DAQ system and the overspeed PLC mentioned in Section 5.9.1.

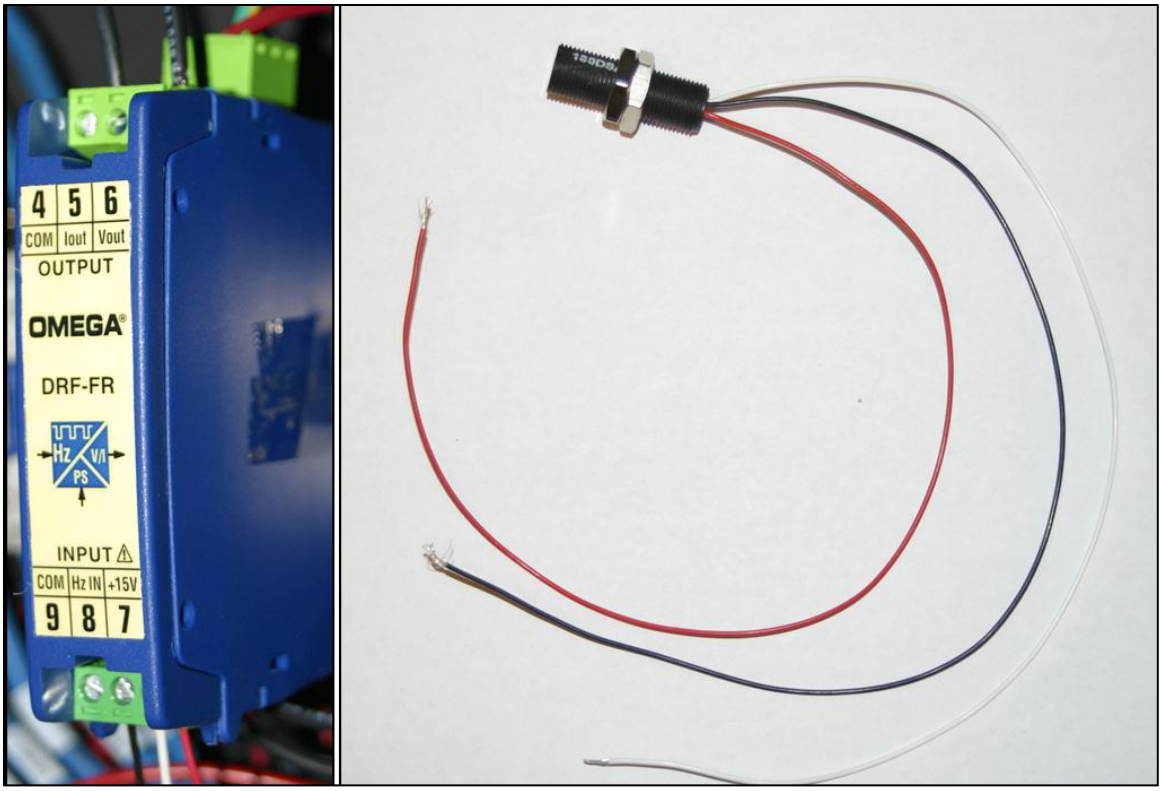

Figure 5-11: Omega Engineering DRF-FR-24VDC frequency to voltage converter and Sensor Solutions Corp. gear tooth sensor.

5.8.5 Water/glycol Flow Meter

The water/glycol flow rate going through the hot side of the vaporizer is measured using a Rosemount 8732C flow meter. This meter is part of the plant control system and reports data to the main LabVIEW host program via a shared variable over an Ethernet connection.

5.9 Safety Systems

5.9.1 Safety Trip System

The safety trip system can be activated by one of four means. Two emergency stop buttons mounted on the main skid serve as the means for any personnel in the

vicinity of the system to trip the safety measures. The DAQ system also has access to the safety system through a 24 VDC digital channel. Additionally, a dedicated Koyo Click C0-02DD20D PLC monitors the speed of the turbine at all times and activates the safety system in the case of an overspeed event via a 24 VDC digital signal. Figure 5-12 shows the overspeed PLC.

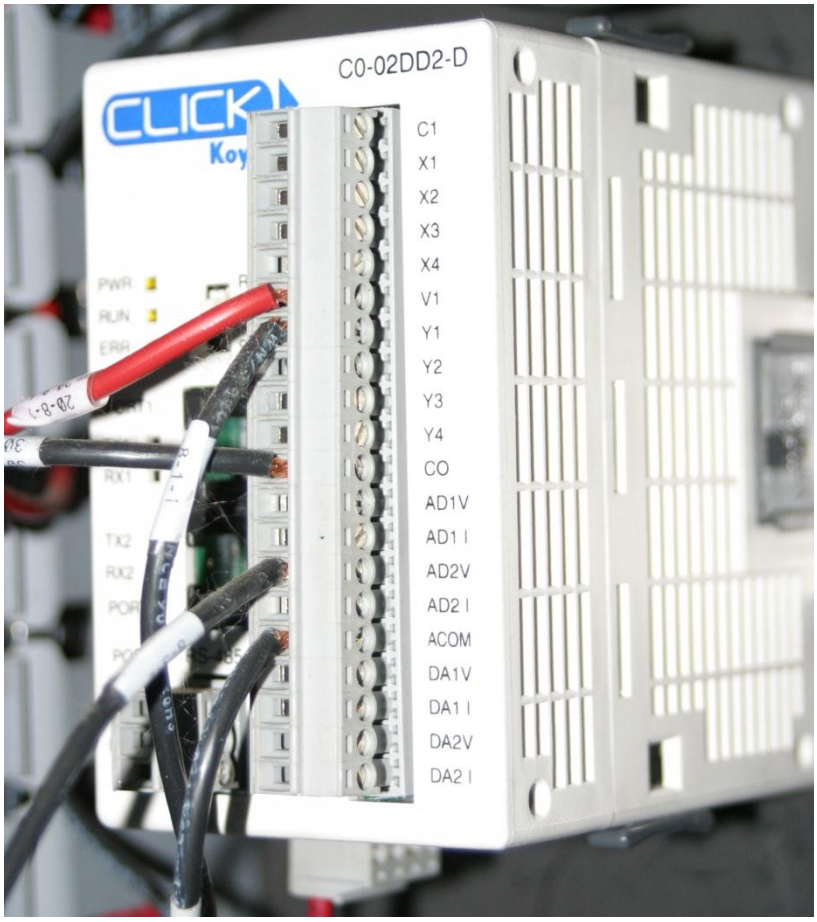

Figure 5-12: Dedicated overspeed PLC, Koyo Click C0-02DD20D.

The safety system, when activated, de-energizes all sources of 480 V power to the main skid via shunt trips on the 480V breakers. Any working fluid flow from the vaporizer to the turbine is directed around the turbine to remove energy flow to the

turbine. This final step is accomplished with a pneumatically actuated 3-way valve that fails to the bypass side when the safety system is activated.

5.9.2 Refrigerant Leak Detection

R245fa is dangerous in high concentrations mainly due to its density being higher than air at atmospheric pressure. Asphyxiation through displacement of oxygen is the main concern. The main skid of the WHR ORC system is situated on the first floor of the EECL. If a leak were to occur, grating nearby allows easy ingress to the basement by the heavier than air R245fa vapors. A Bacharach, 4 Zone HGM-MZ (model 3015-5043) refrigerant leak detection system was installed to ensure the safety of EECL personnel. Three sampling zones are located around the skid on the main floor and one sampling zone is located at ground level in the basement directly below the skid. The efficacy of this system has been tested, due to the leaks in the pump seals mentioned earlier.

5.10 Maintenance System

5.10.1 Carrier Vapormizer 2000

A Carrier Vapormizer 2000 refrigerant recovery system (model 12VA001-100) is used to draw a vacuum on any part of the system and to move refrigerant from one section to another for maintenance. It is also used to move refrigerant from the shipping tanks into the system and from the entire system into the buffer tank where it can be blocked off with valves for storage during long periods of down time. The particular Vapormizer system used contains a GAST model DAA-V137-GB pump. The pump can move refrigerant liquid and vapor without any changes to the hoses or valves.

6. Experimental Procedures

Three main variables of the WHR ORC system are of interest: turbine speed, working fluid flow rate and ambient air temperature at the condenser. All other conditions were to be held constant during experiments, but it was found to not be easily accomplished. During testing of what was supposed to be steady state runs, the working fluid flow rate and water/glycol inlet temperature were fluctuating. However, much was learned about operation of the system and a general conclusion about system performance is made.

6.11 Test Procedures

6.11.1 Preparations

All valves were actuated to the “System Run” configuration as shown in the valve configuration table in Appendix VII. Reference the P&ID in Appendix VI for valve locations in the system. The valve positions direct the entire mass flow rate of water/glycol from the heat source through the ORC vaporizer during testing. Power was applied to all components including the pump and generator VFD, condenser and DAQ system.

The condenser temperature controller was set to 23.9 °C. This setting causes two condenser fans to come on at a condensate exit temperature of 18.3 °C and another

two sequentially at 21.1 °C. During testing, it was visually noted how many fans were on during any data collection point so overall system efficiency calculations could be made.

6.11.2 Heat Source Engine Warm Up

Testing of the WHR ORC system relied on the operation of one of two heat source engines at the EECL. The procedure for warming each of the heat source engines to operating temperature is unique. The Caterpillar G3516 provides a water/glycol temperature of 94 °C and heat flow in excess of the desired 250 kW at standard operating conditions and partial load.

The Waukesha VGF18GL provides 82 °C and 195 kW of energy to the water/glycol at standard full load operating conditions. When the Waukesha was run, the EECL plant control system was set to allow the water/glycol outlet temperature of the engine to reach 90 °C and the engine had to be loaded to its maximum capacity, approximately 300 kW. In either case, the heat source engine was brought up to its full operating temperature and in the case of the Waukesha, fully loaded, before any data was collected from the WHR ORC system.

6.11.3 WHR ORC System Operation

The turbine was driven up to the current test speed by the motor/generator. The bypass valve (V3) was set to direct the R245fa vapor flow to the turbine. The feed pump was started and increased in speed until the turbine inlet pressure was the same as the vapor saturation pressure of R245fa at 5°C below the water/glycol inlet temperature or the system maximum pressure of 0.97 MPa was reached. Once steady-state was

reached, the temperature of the R245fa vapor entering the turbine was checked to ensure full saturation. If the vapor was being superheated or not reaching full saturation, pump speed was increased or decreased accordingly. When the steady state was reached, the pump was pushing fully saturated R245fa vapor against the fixed geometry of the turbine nozzles.

In all tests, the VFD is set to control turbine speed, and initially the VFD drives the generator as a motor, driving the turbine. When the turbine begins to produce power, it accelerates the motor slightly, the generator VFD automatically switches to regeneration to maintain the set point speed. Temperatures , working fluid flow rate and power generation values were allowed to stabilize and 2 minutes of data were taken.

Once the data point was taken, the turbine was ramped to the next test speed, the system allowed to stabilize and another 2 minute data point taken.

7. Results and Discussion

Due to several mechanical difficulties with the pump and a lack of scheduled heat source engine run days throughout the period of this study, only one test day was successful in running a turbine speed sweep.

7.1 Commissioning: June 2011

Low power test runs of the WHR ORC system were conducted in June 2011. The building boiler at the EECL was used as the heat source. The purpose of these tests were to work out any control, date logging or equipment issues before one of the heat source engines was run.

7.1.1 Commissioning Results

The turbine could not be adequately tested as it only ran at 300 RPM on the reduced heat flow and water/glycol temperature from the boiler. However, it was observed that even though the working fluid flow rate was kept constant, severe system oscillations were occurring. The oscillations were noticed because the pump would cycle between running dry and pumping liquid.

It was discovered the fans on the condenser were cycling on and off. This was caused by an overshoot response from the condenser and its fan controller. As the temperature of the condensate increased, all 4 fans would be turned on. The

condensate temperature would decrease and the working fluid would condense and pool in the condenser. This would cause the pump to run dry. The condensate would eventually cool enough because energy was not being sent to the condenser and the fans would turn off. The condensate would run out of the condenser and into the buffer tank. The pump would then begin to pump liquid again and the oscillation would repeat with the system never reaching steady state.

This behavior indicated the need to carefully watch the condenser fans during testing and control the fans manually if this behavior occurred. A future improvement to the WHR ORC system would be to allow the DAQ system to control the condenser fans. The fans could be cycled based on more process variables than just the condensate return temperature.

7.2 Testing Day 1: July 21, 2011

Modeling by Toucan Design Inc. set the operating speed of the turbine at a maximum of 3600 RPM based on the turbine's nozzle geometry and the speed of sound in R245fa at the design conditions. For this reason, the system was designed around a 1:1 belt ratio with a 3600 RPM motor. The Caterpillar G3516C was the heat source engine and an ambient temperature at the condenser of 30 °C was observed. All four condenser fans ran throughout all data collection.

Mark Toukan of Toucan Design Inc. was present for testing. It became apparent to Mark when running the turbine at the maximum set point of 3600 RPM, the nozzles of the turbine where not performing as expected and the turbine could run faster and more efficiently. At the recommendation of Mr. Toukan, the WHR ORC system was shut

down and the belt connecting the turbine to the generator removed. This would allow the turbine to free spool to over 3600 RPM without damaging the generator and let Mark get a better sense of where the turbine wanted to run.

Upon restarting the ORC, the turbine reached a maximum speed of approximately 10,000 RPM. This speed was measured with a laser tachometer as the frequency to voltage converted installed at the time could not interpret speeds above 5000 RPM. With the belt removed, there was no means to load the turbine and collect useful performance data.

7.2.1 Testing Day 1 Results

1. The turbine could not spin fast enough to run “where it wanted to” with a 1:1 turbine to generator belt ratio without risking damage to the generator
2. The pump’s pressure relief valve would not let the pump develop the differential pressure required to operate at the designed pressures
3. The hand built frequency to voltage converter was malfunctioning and not reading accurate speeds as checked by a laser tachometer.

As a consequence of issue (1) above, the belt ratio was modified to 3:1. The bearings on the turbine secondary shaft were also replaced with Sealmaster NPL-16T bearings as the original ones were rated to 5000 RPM. Each NPL-16T has a L10, 50000 hour rating at 8000 RPM and 44.9 kg load. The shaft the bearings support is subject to a 87.3 kg load from the belt. Short periods over 8000 RPM during future testing were deemed non-detrimental to the bearings as heat buildup is the primary cause of failure in this application.

Issue (2) from above can be observed from the data shown in Figure 7-1. This was resolved by installing a stiffer relief valve spring in the pump, Blackmer part number 471428. The pump was then capable of producing a pressure differential of 1.03 MPa.

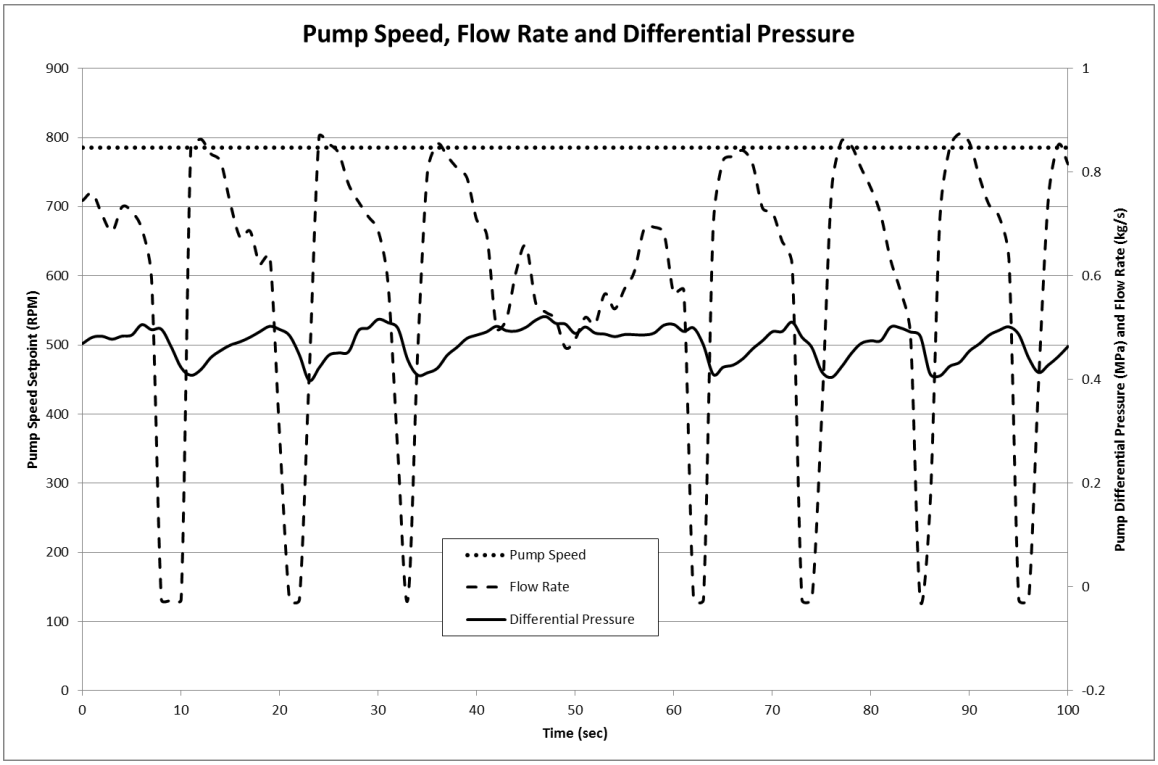

Figure 7-1: Pump Speed, Flow Rate and Differential Pressure. Note differential pressure peaking at 0.5 MPa and flow rate dropping repeatedly while pump speed is constant. This indicates the pressure relief valve was opening repeatedly.

Issue (3) was solved by replacing the hand built frequency to voltage converter with an Omega Engineering DRF-FR-24VDC mentioned in Section 5.8.4.

7.3 Testing Day 2: Oct 21, 2011

The heat source for test day 2 was the Waukesha VGF18GL. The engine was run at the maximum load of 300 KW and the building control system was set to allow the engine to run at a water/glycol outlet temperature of 90 °C. The ambient air

temperature range was 22.8-20.5 °C. All 4 fans of the condenser were running during data collection with the condenser fan controller set at 23.9 °C.

7.3.1 Testing Day 2 Results

1. During testing the pump was not producing the pressure and correlated flow rate required to move the turbine inlet point on a P-h diagram to the vapor saturation line. The vapor was exiting the vaporizer superheated. The pump speed command was increased with no associated increase in flow rate or pressure. Eventually, the motor overheated and shut off.
2. The water/glycol inlet temperature to the vaporizer was not stable during testing.
3. The post processed data showed the unrealistic result that enthalpy was increasing from the inlet to exit of the turbine while the turbine was generating power.
4. It was shown the exit pressure at the condenser was within 0.007 MPa of the inlet to the pump.
5. A system relative efficiency to turbine RPM plot was obtained.

Issue (1) above was assumed to be caused by the pump motor slipping excessively. All alternating current induction motors experience some amount of slip. As load is increased slip and motor heating increase, in this case, to the point of motor shutdown. Studying the pump VFD manual revealed the VFD possessed an automatic slip compensation system, but was not activated during testing. To solve the slip problem, slip compensation was enabled on the pump VFD.

The solution to issue (2) above was to more closely watch the vaporizer inlet temperature. If the temperature begins to deviate the WHR ORC system operator

should converse with the engine operator to determine why the temperature is not remaining constant even though the heat source engine power output is constant.

In an attempt to solve the problem with unrealistic enthalpy values, a system of valves, tubing and two additional thermocouples were added upstream and downstream of the turbine to allow the establishment of fluid state further away from the turbine. There are two hypotheses of why an enthalpy increase was observed.

The first hypothesis is that a velocity effect exists within the turbine causing the pressure transducers to measure dynamic pressure instead of static pressure. The valves and additional tubing allow the pressure transducers at the inlet and outlet of the turbine to measure pressure further upstream and downstream of the turbine in an attempt to remove any effects from the fluid velocity in the turbine.

The second hypothesis has to do with the proximity of the turbine exhaust thermocouple to the turbine output shaft flex coupler. It was noted after testing the coupler was relatively hot to the touch, hotter than the turbine casing. The exhaust thermocouple is 50mm from the coupler. It is plausible the thermocouple was being artificially heated by the coupler.

Result 4 was significant because during system design, it was assumed the outlet of the condenser was at the same pressure as the inlet of the pump. With the final placement of the condenser being on the third floor roof with almost 20 m of pipe between the main skid and itself, the need to check the validity of the assumption was required. A manual pressure gauge was installed at the outlet of the condenser and the assumption was confirmed with result 4.

The system was not stable during the sweep from a turbine speed of 2000 RPM to 6500 RPM before the pump shutdown from overheating. Despite the unsteady system, a relative performance curve could be established and is shown in Figure 7-2. System performance is calculated according to equation (7.1):

$$\eta = \frac{\dot{W}_{exp} - \dot{W}_p - \dot{Q}_f}{\dot{Q}_{vap}} \tag{7.1}$$

where $\dot{W}_{exp}$ and $\dot{W}_p$ is the work done by the expander and consumed by the pump respectively, $\dot{Q}_f$ is the energy consumed by the condenser fans and $\dot{Q}_{vap}$ is the energy input to the working fluid in the vaporizer. All four condenser fans were assumed to be consuming their full 0.75 kW, likely a conservative assumption.

During this test, the system was consuming more power than it was producing, hence the negative efficiency numbers. Also, the efficiency of the pump and motor VFD were not taken into account. The important result is that even with flow rate and turbine inlet temperature generally decreasing, system efficiency still increased from 2000 to 400 RPM. As mentioned previously, ORC system efficiency is strongly tied to expander efficiency. From this plot, the hypothesis that future testing with reveal that the turbine will run most efficiently near 4000 RPM can be made.

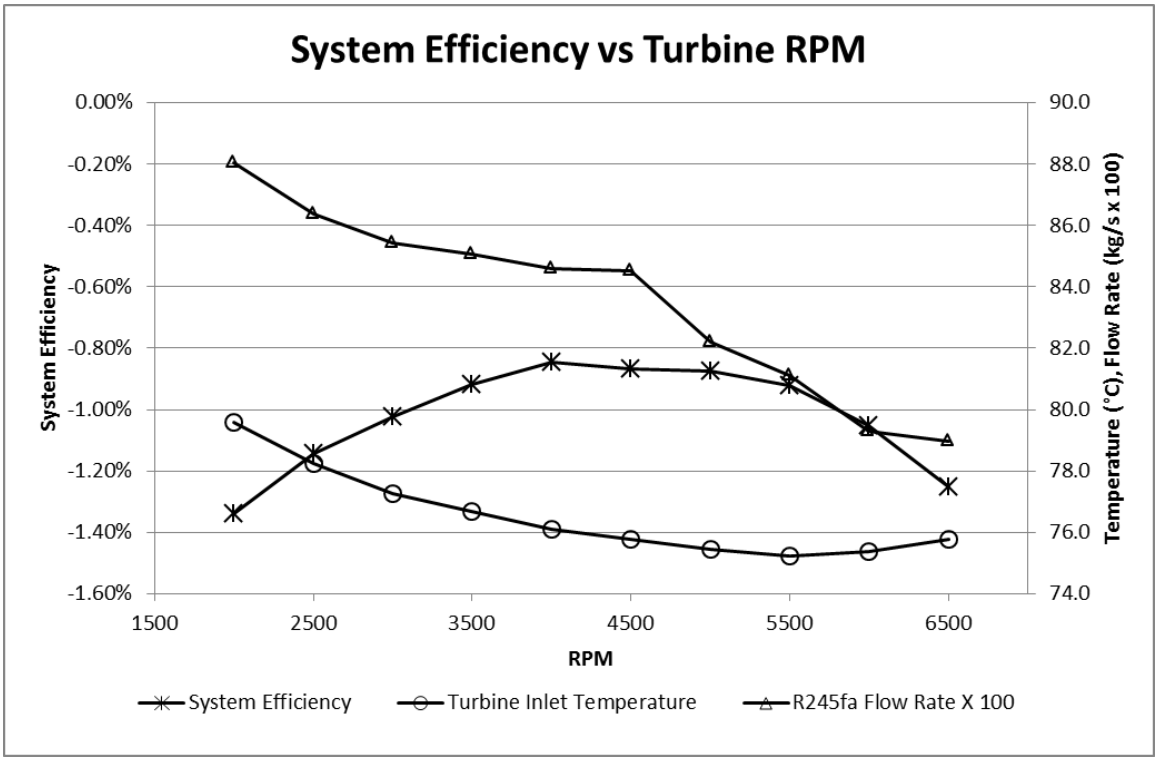

Figure 7-2: System efficiency versus turbine RPM. Negative efficiency indicates the system was consuming more power than it was producing. The general shape of the efficiency curve is important indicating the turbine's highest efficiency is near 4000 RPM.

8. Conclusions

A Waste Heat Recovery Organic Rankine Cycle test bed utilizing dry cooling and R245fa as the working fluid was designed constructed and commissioned. A Tesla-hybrid turbine from Toucan Design Inc. was used as the expander. In each subsequent run of the test bed, changes were made to the system so future experiments would produce more conclusive results. The final experiment has given the preliminary result the system and turbine will run most efficiently near 4000 RPM.

8.1 Recommendations For Future Work

Due to a lack of test days during this work, it is recommended that additional data be taken with the Toucan Design Inc. Tesla-hybrid turbine on the EECL WHR ORC test bed. The Tesla-hybrid turbine has shown great potential as a robust expander in tests on steam. The preliminary results from this work while operating the turbine on an organic fluid are promising. The turbine should be completely characterized through a realistic range of inlet and outlet conditions and rotational speeds.

After the last test in this work, a system of valves was installed to allow measurement of pressure further upstream and downstream of the turbine. All future tests should measure the working fluid temperature and pressure at the turbine, then the valves should be actuated so pressure can be measured at the upstream and downstream locations. This serves to potentially solve the increasing turbine enthalpy issue.

The main control system for the ORC should be controlling the fans on the condenser. This would allow fan cycling based on more process variables than just the condensate return temperature. This would also eliminate the need to visually confirm which fans are active during testing.

Power meters installed on the feed pump, generator and condenser 480 V, 3 phase power lines would result in extremely accurate system efficiency calculations and should be considered. Also, a torque senor should be installed on the turbine to allow calculation of actual turbine power output without including belt drive and power conversion losses.

One of the overarching goals for the test bed is to conduct research on different expanders and working fluids while working at varying condenser conditions. Especially interesting would be to study the performance of variable displacement expanders with varying condenser temperatures and pressures. This would serve to verify the MATLAB model developed in [46].

Since this work started, at least one new working fluid, Solkatherm, has been realized. It has also been noticed that Honeywell is working on an ultra-low ODP and GWP working fluid that potentially exhibits higher system efficiencies than R245fa [54]. Running these new fluids in the WHR ORC system is recommended if funds allow.

A mechanical change that should be executed is installation of more robust flange gaskets. The gaskets originally installed are solid PTFE. PTFE gaskets are known to cold creep over time and could eventually leak if a regular flange torqueing routine is not carried out.

The Blackmer vane pump should be replaced with something more robust that does not rely on mechanical face seals or o-rings. The Blackmer SGL vane pump sealing system does not work well with Teflon o-rings, supposedly due to the harder durometer of Teflon. The pump leaked from the factory. The leak was corrected by installing standard HNBR o-rings. HNBR is not listed as compatible with R245fa, however, discussions with Honeywell indicated they should not break down at temperatures near the 50 °C the pump would see in the WHR ORC system. The pump developed a second leak after the first rebuild and required another rebuild requiring replacement of the rotor and shaft assembly. Overall, the Blackmer pump is the weak point of the WHR ORC system and should be replaced. Initial quotes of a suitable diaphragm pump came in at $7,000 USD.

A final recommendation for future work on the WHR ORC system is to secure funding for running one of the two heat source engines. Tests on the WHR ORC system were extremely limited during the period of this study due to limited heat source engine run days for other projects.

9. References

[1] World Energy Council, 2011, "WEC Issues Surveys 2011 - The Global Energy Agenda."

[2] Kreis S., 2011, "Waste Heat Recovery Gains Attention in the US," IHS Inc., Report #NARP 815-110112.

[3] Johnson I., and Choate W. T., 2008, "Waste Heat Recovery : Technologies and Opportunities in the U.S. Industry," BCS, Inc.

[4] Barber R. E., 1978, "Current Costs of Solar Powered Organic Rankine Cycle Engines," Solar Energy, 20(1), pp. 1-6.

[5] Larjola J., 1995, "Electricity from Industrial Waste Heat Using High-speed Organic Rankine Cycle (ORC)," International Journal of Production Economics, 41(1-3), pp. 227-235.

[6] Hung T. C., Shai T. Y., and Wang S. K., 1997, "A Review of Organic Rankine Cycles (ORCs) for the Recovery of Low-grade Waste Heat," Energy, 22(7), pp. 661-667.

[7] Hung T. C., Wang S. K., Kuo C. H., Pei B. S., and Tsai K. F., 2010, "A Study of Organic Working Fluids on System Efficiency of an ORC Using Low-grade Energy Sources," Energy, 35(3), pp. 1403-1411.

[8] Liu B.-T., Chien K.-H., and Wang C.-C., 2004, "Effect of Working Fluids on Organic Rankine Cycle for Waste Heat Recovery," Energy, 29(8), pp. 1207-1217.

[9] Radermacher R., 1989, "Thermodynamic and Heat Transfer Implications of Working Fluid Mixtures in Rankine Cycles," International Journal of Heat and Fluid Flow, 10(2), pp. 90-102.

[10] Saleh B., Koglbauer G., Wendland M., and Fischer J., 2007, "Working Fluids for Low-temperature Organic Rankine Cycles," Energy, 32(7), pp. 1210-1221.

[11] Badr O., Probert S. D., and O'Callaghan P. W., 1985, "Selecting a Working Fluid for a Rankine-Cycle Engine," Applied Energy, 21(1), pp. 1-42.

[12] Ganic E. N., and Wu J., 1980, "On the Selection of Working Fluids for OTEC Power Plants," Energy Conversion and Management, 20(1), pp. 9-22.

[13] Marcuccilli F., and Thiolet D., 2010, "Optimizing Binary Cycles Thanks to Radial Inflow Turbines," World Geothermal Congress 2010, Bali, Indonesia.

[14] Facao J., and Oliveira A. C., 2009, "Analysis of Energetic, Design and Operational Criteria When Choosing an Adequate Working Fluid for Small ORC Systems," 2009 International Mechanical Engineering Congress & Exposition, Paper #IMECE2009-12420, ASME, Lake Buena Vista, FL, USA.

[15] Buchanan T., Posten W., and Berryman S., 2010, “Repowering Steamboat 2 and 3 Plants with New Axial Flow Turbines,” World Geothermal Congress 2010, Bali, Indonesia.
[16] Quoilin S., and Lemort V., 2009, “Technological and Economical Survey of Organic Rankine Cycle Systems,” 5th European Conference Economics and Management of Energy in Industry, Algarve, Portugal.
[17] Nelson C. R., 2006, “Achieving High Efficiency at 2010 Emissions,” DEER Conference 2006, Detroit, MI.
[18] Teng H., 2010, “Waste Heat Recovery Concept to Reduce Fuel Consumption and Heat Rejection from a Diesel Engine,” SAE International Journal of Commercial Vehicles, 3(1), pp. 60 -68.
[19] Freymann R., Strobl W., and Obieglo A., 2008, “The Turbosteamer-A System Introducing the Principle of Cogeneration in Automotive Applications,” MTZ, 69, pp. 20-27.
[20] Endo T., Kawajiri S., Kojima Y., Takahashi K., Baba T., Ibaraki S., Takahashi T., and Shinohara M., 2007, “Study on Maximizing Exergy in Automotive Engines,” Paper# 2007-01-0257, SAE International, Detroit, MI.
[21] Oomori H., and Ogino S., 1993, “Waste Heat Recovery of Passenger Car Using a Combination of Rankine Bottoming Cycle and Evaporative Engine Cooling System,” Paper# 930880, SAE International, Detroit, MI.
[22] Lemmon E. W., Huber M. L., and McLinden M. O., REFPROP, NIST.
[23] Fröba A. P., Kremer H., Leipertz A., Flohr F., and Meurer C., 2007, “Thermophysical Properties of a Refrigerant Mixture of R365mfc (1,1,1,3,3-Pentafluorobutane) and Galden® HT 55 (Perfluoropolyether),” International Journal of Thermophysics, 28, pp. 449-480.
[24] Johnston J. R., 2001, “Evaluation of Expanders for Use in a Solar-powered Rankine Cycle Heat Engine,” thesis, The Ohio State University, Columbus, OH.
[25] Badr O., O’Callaghan P. W., and Probert S. D., 1984, “Performances of Rankine-cycle Engines as Functions of Their Expanders’ Efficiencies,” Applied Energy, 18(1), pp. 15-27.
[26] Biddle R., November, “Exploiting Wasted Heat: New Approaches to Electricity Generation from Wasted Heat,” Refocus, 6(6), pp. 34-37.
[27] Badr O., O’Callaghan P. W., Hussein M., and Probert S. D., 1984, “Multi-vane Expanders as Prime Movers for Low-grade Energy Organic Rankine-cycle Engines,” Applied Energy, 16(2), pp. 129-146.
[28] Musthafah M.-T., Yamada N., and Hoshino T., 2010, “Efficiency of Compact Organic Rankine Cycle System with Rotary-Vane-Type Expander for Low-Temperature Waste Heat Recovery,” International Journal of Civil and Environmental Engineering, 2(1), pp. 11-16.
[29] Badr O., Naik S., O’Callaghan P. W., and Probert S. D., 1991, “Expansion Machine for a Low Power-output Steam Rankine-cycle Engine,” Applied Energy, 39(2), pp. 93-116.

[30] Ng K. C., Bong T. Y., and Lim T. B., 1990, "A Thermodynamic Model for the Analysis of Screw Expander Performance," Heat Recovery Systems and CHP, 10(2), pp. 119-133.
[31] Mathias J. A., Johnston J., Cao J., Priedeman D. K., and Christensen R. N., 2009, "Experimental Testing of Gerotor and Scroll Expanders Used in, and Energetic and Exergetic Modeling of, an Organic Rankine Cycle," J. Energy Resour. Technol., 131(1), pp. 012201-9.
[32] Lemort V., Quoilin S., Cuevas C., and Lebrun J., 2009, "Testing and Modeling a Scroll Expander Integrated into an Organic Rankine Cycle," Applied Thermal Engineering, 29(14-15), pp. 3094-3102.
[33] Hayter M., 2008, "Raser Technolgies, Inc Overview Presentation," http://geology.utah.gov/emp/geothermal/ugwg/geothermal0408/pdf/hayter0408.pdf.
[34] Tchanche B. F., Quoilin S., Declaye S., Papadakis G., and Lemort V., 2010, "Economic Feasibility Study of a Small Scale Organic Rankine Cycle System in Waste Heat Recovery Application," 10th Biennial Conference on Engineering Systems Design and Analysis, Paper #ESDA2010-24828, ASME, Istanbul, Turkey.
[35] Galanis N., Cayer P. R., Denis E. S., and Desilets M., 2009, "Electricity Generation from Low Temperature Sources," Journal of Applied Fluid Mechanics, 2(2), pp. 55-67.
[36] Heydt G. T., 1993, "An Assessment of Ocean Thermal Energy Conversion as an Advanced Electric Generation Methodology," Proceedings of the IEEE, 81(3), pp. 409-418.
[37] Kalina J., 2010, "Integrated Biomass Gasification Small-Scale Combined Cycle Distributed Generation Plant With Microturbine and ORC," ASME Conf. Proc., 2010(43949), pp. 503-514.
[38] Cong C. E., Sanjayan V., and Darus A. N., 2005, "Solar Thermal Organic Rankine Cycle as a Renewable Energy Option," Jurnal Mekanikal, (20), pp. 68-77.
[39] Holdmann G., Test Evaluation of Organic Rankine Cycle Engines Operating on Recovered Heat from Diesel Engine Exhaust, Alaska Center for Energy and Power.
[40] Patel P. S., and Doyle E. F., 1976, "Compounding the Truck Diesel Engine with an Organic Rankine-Cycle System," Automotive Engineering Congress and Exposition, Paper #760343, SAE International, Warrendale, PA.
[41] Vaja I., and Gambarotta A., 2010, "Internal Combustion Engine (ICE) bottoming with Organic Rankine Cycles (ORCs)," Energy, 35(2), pp. 1084-1093.
[42] El Chammas R., and Clodic D., 2005, "Combined Cycle for Hybrid Vehicles," 2005 SAE World Congress, Paper # 2005-01-1171, SAE International, Warrendale, PA.
[43] Doyle E., Dinanno L., and Kramer S., 1979, "Installation of a Diesel-Organic Rankine Compound Engine in a Class 8 Truck for a Single-Vehicle Test," Passenger Car Meeting, Paper #790646, SAE International, Warrendale, PA.
[44] Srinivasan K. K., Mago P. J., and Krishnan S. R., 2010, "Analysis of Exhaust Waste Heat Recovery from a Dual Fuel Low Temperature Combustion Engine Using an Organic Rankine Cycle," Energy, 35(6), pp. 2387-2399.

[45] Johnson K. M., Testimony on the U.S. Department of Energy's (DOE's) Programs for Developing Water-efficient Environmentally-sustainable Energy-Related Technologies.
[46] Zimmerle D., and Cirincione N., 2011, "Analysis of Dry Cooling for Organic Rankine Cycle Systems," 5th International Conference on Energy Sustainability, Paper #ESFuelCell2011-54202, ASME, Washington, DC, USA.
[47] Badr O., Probert S. D., and O'Callaghan P. W., 1985, "Multi-vane Expanders: Internal-Leakage Losses," Applied Energy, 20(1), pp. 1-46.
[48] Tesla N., 1913, "Turbine."
[49] Rey A. F., 2007, "Numerical Simulation of the Flow Field in a Friction-Type Turbine (Tesla Turbine)," Institute of Thermal Powerplants Vienna University of Technology.
[50] Hoya G. P., and Guha A., 2009, "The Design of a Test Rig and Study of the Performance and Efficiency of a Tesla Disc Turbine," Proceedings of the Institution of Mechanical Engineers, Part A: Journal of Power and Energy, 223(4), pp. 451-465.
[51] Guha A., and Smiley B., 2010, "Experiment and Analysis for an Improved Design of the Inlet and Nozzle in Tesla Disc Turbines," Proceedings of the Institution of Mechanical Engineers, Part A: Journal of Power and Energy, 224(2), pp. 261 -277.
[52] Rice W., 1965, "An Analytical and Experimental Investigation of Multiple-Disk Turbines," Journal of Engineering for Power, 87(1), pp. 29-36.
[53] Armstrong J., 1952, "An Investigation of the Performance of a Modified Tesla Turbine," Georgia Institute of Technology.
[54] Zyhowski G., and Brown A., 2011, "Low Global Warming Fluids for Replacement of HFC-245fa and HFC-134ain ORC Applications."

Appendix I- REFPROP Excel Model Spreadsheet

Constants

Working Fluid	R245fa	
Units	C	
Condenser Temp	50	C
Boiler Temp	85	C
Boiler Input Power	250	KW
Turbine Isentropic Efficiency	75%	
Pump Isentropic Efficiency	75%	

Organic Rankine Cycle Simulation

Outlet of	Inlet of	State	Temperature (°C)	Pressure (MPa)	Enthalpy (KJ/Kg)	Entropy (KJ/Kg-K)	Quality
Condenser	Pump	1	50	0.344	266.3	1.222	0
Pump	Boiler	2	50.3	0.893	266.9	1.222	0
Boiler	Expander	3	85.0	0.893	465.0	1.783	1
Expander	Condenser	4	60.5	0.344	451.9	1.796	1

Summary Output

Flow Rate (Kg/s)	1.26
Volumetric Flow Rate (m^3/sec)	0.00099
Pump Input Power (KW)	0.73
Jacket Input Power (KW)	250.00
Expander Output Power (KW)	16.5
Net Power with pump (KW)	15.8
Condenser Fan Power (KW)	3.0
Condenser Output Power (KW)	234.2
Cycle Efficiency	5.1%

Appendix II - AspenTech Aspen Plus Annotated Flowsheet

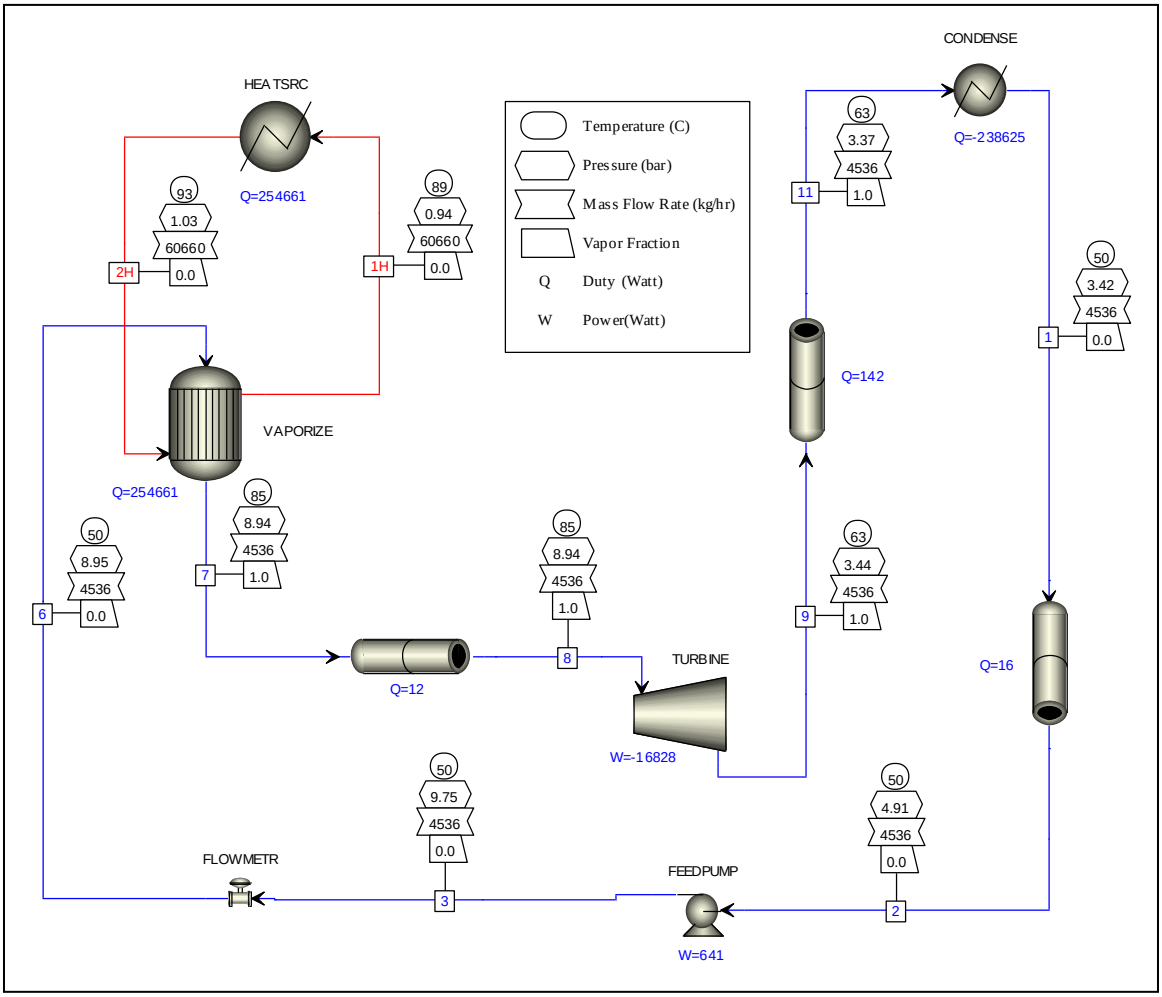

Appendix III - Pro-E Model

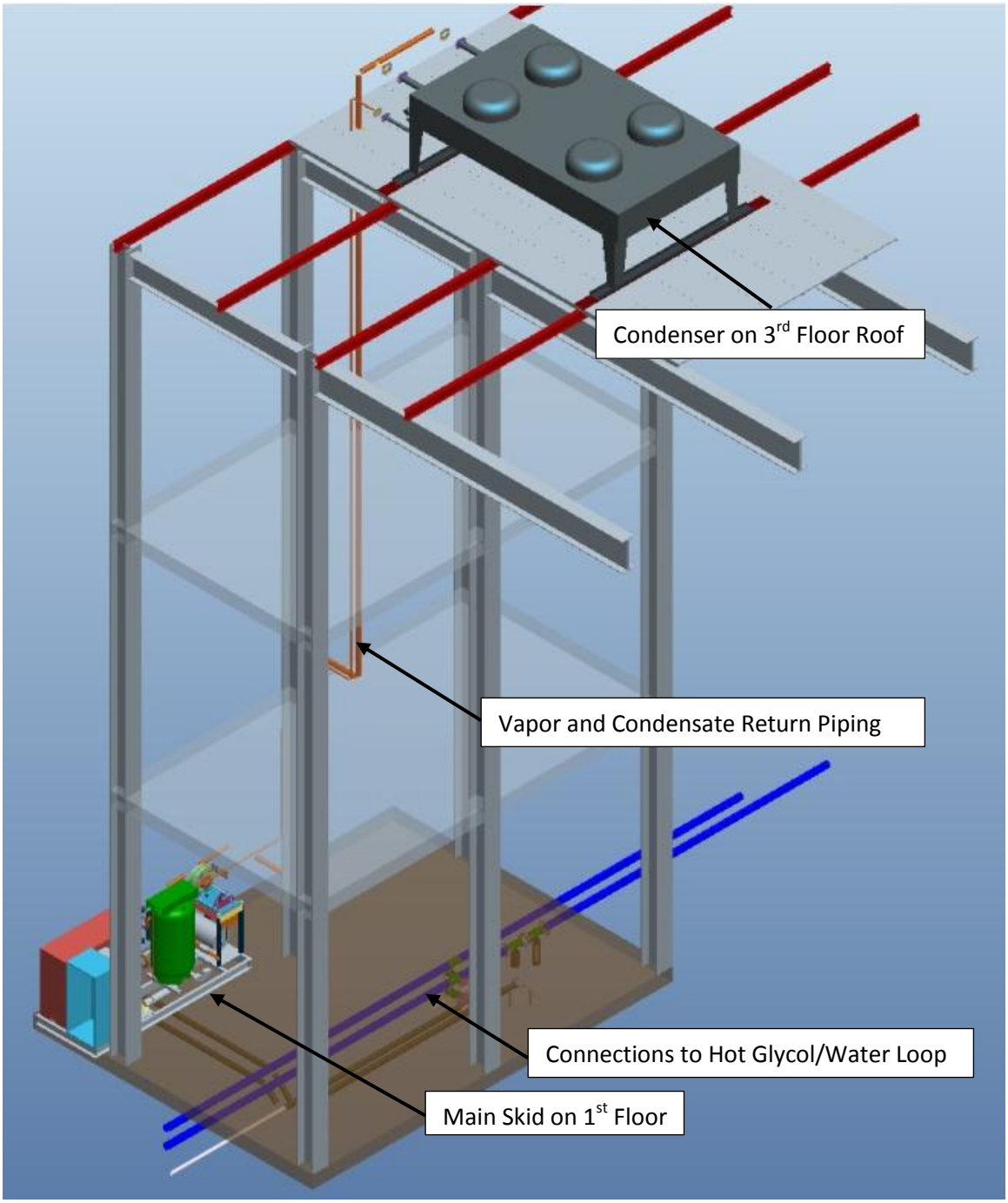

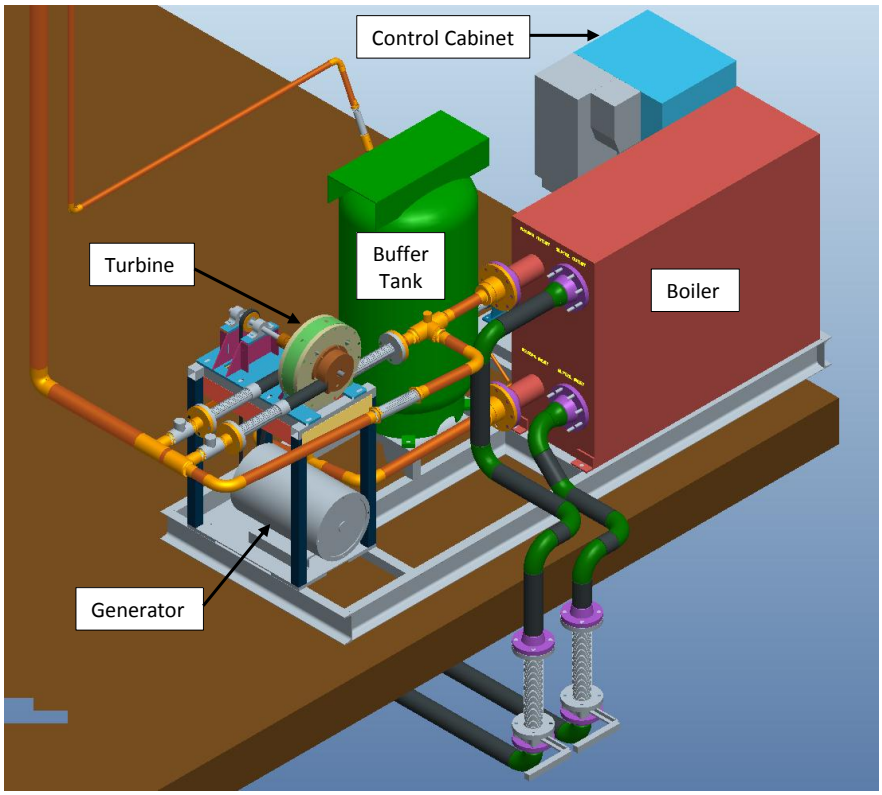
Control Cabinet
Turbine
Buffer Tank
Boiler
Generator

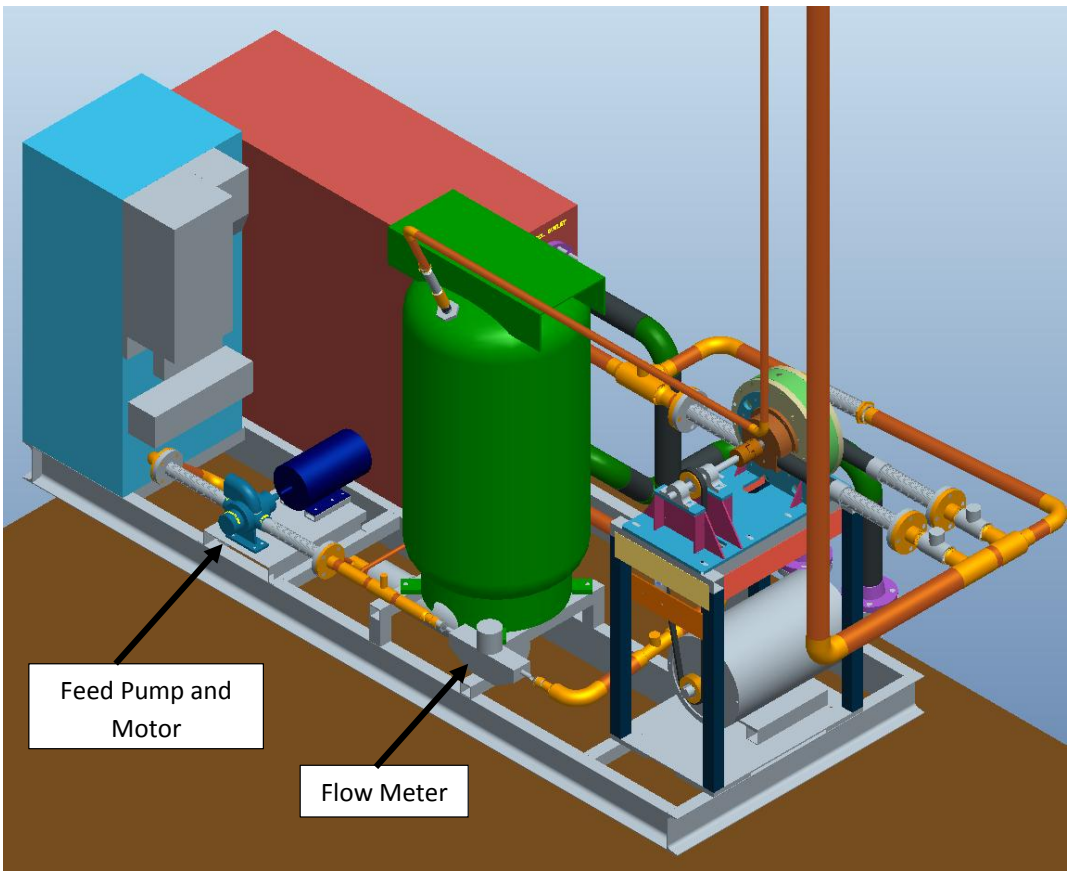
Feed Pump and Motor
Flow Meter

Appendix IV - Vaporizer Specifications

ITT Standard Plate and Frame Heat Exchanger Specification Sheet
www.ittstandard.com

Quotation No.: 138611 rev 1 Item No.: 02 Date: 11/05/2009
Model: WP26A Version: 1.0.0.87

	Side 1		Side 2	
Fluid Name	R245FA		PropGlycol - 50%	
Total Flow	2.78	(Lb/s)	268.0	(g.p.m.)
Inlet Temperature	50.0	(°F)	199.4	(°F)
Outlet Temperature	185.0	(°F)	190.4	(°F)
Pressure Drop, (calc)	0.5	(PSI)	4.0	(PSI)
Density			61.86	(Lb/Ft³)
Mean Viscosity			0.99	(cP)
Wall Viscosity			1.09	(cP)
Specific Heat			0.91	(Btu/Lb*F)
Thermal Conductivity			0.22	(Btu/h*Ft*F)

Total Heat Exchanged 1,087,200(Btu/h)

Plate Arrangement	1 x 59	1 x 60
Number of Plates (Total/Max)	120	152
Pressure Design/Test	150.00 (PSI)	195.00 (PSI)
Design Temperature	257 (°F)	257 (°F)
Est. Weight (Empty/Operating)	1400 LBS	1550 LBS

Side-1 Inlet Connection	(F4) 4 inch steel weld end
Side-1 Outlet Connection	(F1) 4 inch steel weld end
Side-2 Inlet Connection	(F3) 4 inch Unlined studded port for 150# ANSI flg
Side-2 Outlet Connection	(F2) 4 inch Unlined studded port for 150# ANSI flg
Frame Size	1300 mm
Total Heat Transfer Surface Area	363.3 (Ft²)
Total Internal Volume	2.4 (Ft³)
Plate Material/Thickness	AISI316 / 0.6 mm
Plate Mix	TL
Gasket Material	NITRIL/EPDM RING TEFLON

Approvals: none

Appendix V- Condenser Specifications

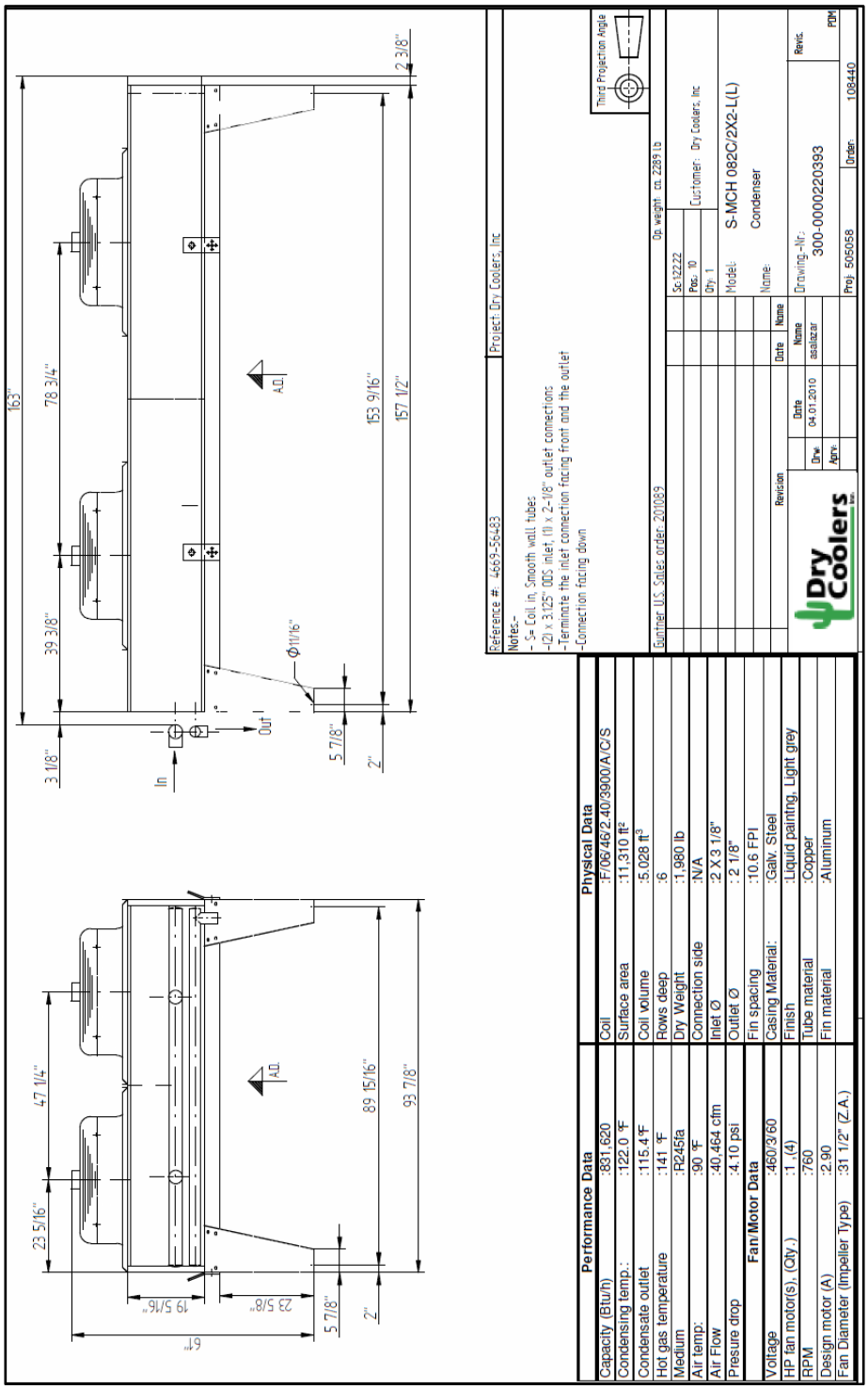

Appendix VI - Piping and Instrumentation Diagram

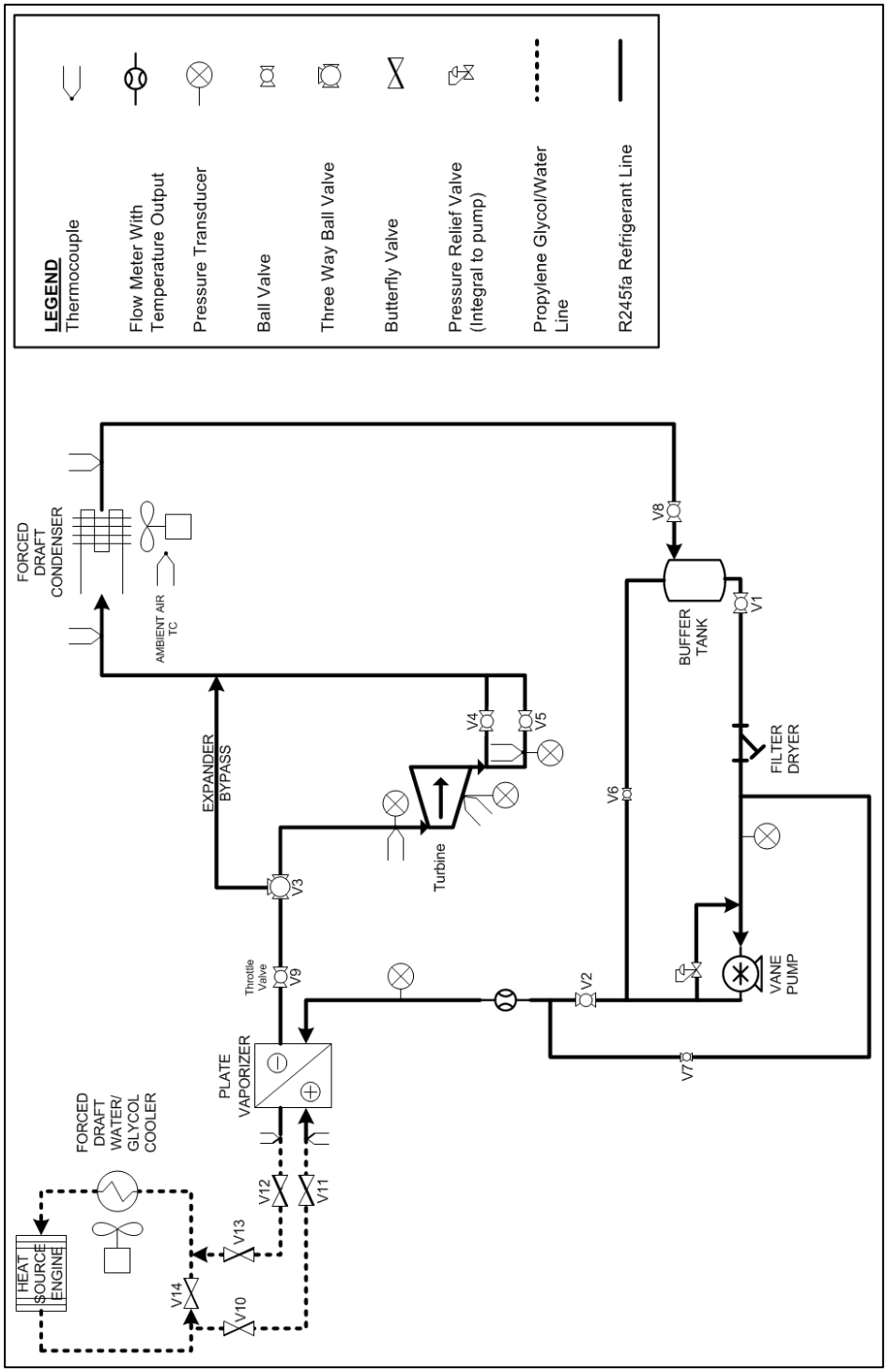

Appendix VII - Valve Configuration Table

Configuration Table: Refrigerant									
Task	V1 1.5" filter inlet	V2 1.5" pump outlet	V3 (3 way) 2" Bypass*	V4 2" Turbine outlet 1	V5 2" turbine outlet 2	V6 1" Vertical pump bypass	V7 1" Horizontal pump bypass	V8 1" From condenser	V9 2" Exit of HE
Change Filter	c	c	Closed	c	c	c	c	c	o
Charge System	o	o	Closed	c	c	o	o	o	o
Discharge system (Evaporate System)	o	c	Open	o	o	c	c	c	o
Discharge system (Fill Buffer)	c	c	Open	o	o	o	o	c	o
Discharge system (Vapor Fill Buffer)	c	o	Open	o	o	c	c	c	o
Initial Start Up	o	o	Closed	o	o	c	c	o	c
Isolate Condenser	c	o	Open	c	c	o	o	c	o
Isolate Filter	c	c	Closed	c	c	o	c	c	c
Isolate Heat Exchanger	o/c	c	Closed	c	c	o/c	c	c	c
Isolate Pump	c	c	Closed	c	c	c	c	c	o
Isolate Suge Tank (Initial)	o	o	Closed	c	c	c	c	c	o
Isolate Surge Tank (Final)	c	o	Closed	c	c	c	o	c	o
Isolate Turbine	o	o	Closed	c	c	o	o	o	o
System Run	o	o	Open	o	o	c	c	o	o
Vacuum Air Out	o	o	Open	o	o	o	o	o	o

*Closed indicates flow is directed away from the turbine, Open indicates flow is directed to the turbine

Configuration Table: Water/Gycol Loop					
Task	V10 3" Glycol inlet	V11 3" Glycol inlet to HE	V12 3" Glycol exit HE	V13 3" Glycol exit	V14 4" Main
Isolate Glycol Loop	c	c	c	c	o
Isolate Heat Exchanger	c	c	c	c	o
System Run	o	o	o	o	c